

Check for updates

Effective Sliding Motions of Vibration-Induced Emission Stoppers in Mechanically Interlocked Molecules as Artificial Muscle Tougheners and In Situ Molecular Shuttling Sensors for Self-Healable Mechano-Fluorescent Polyurethane Organogels

Tu Thi Kim Cuc, Yu-Chen Lai, Trang Manh Khang, Wei-Tsung Chuang, Tung-Kung Wu, Ricardas Rotomskis, Simona Steponkiene, and Hong-Cheu Lin*

The highly tough, self-healable, and adhesive polyurethane (PU) organogels with force-regulated ratiometric emission switching behaviors are fabricated through covalently linked cellulose nanocrystals (CNCs) as multiple hydrogenbonded crosslinkers and N,N'-diphenyl-dihydrodibenzo[a,c]phenazine (DPAC)modified mechanically interlocked molecules (MIMs) as artificial molecular muscles, including [2]rotaxanes (before/after shuttling) and extended/ contracted [c2] daisy chain molecules with different sliding motions. Interes tingly, the optimal PU organogel consisting of a small amount (ca. 1.5 wt.%) of the first DPAC-based unconventional daisy chain with the particular macrocycle-exerted force mode reveals an admirable toughness of 142 MJ m⁻³, which is ca. 1.6 and 2.6 times higher than the PU organogels containing [2]rotaxane and without MIMs, respectively. Besides, ratiometric mechano-fluorescence responses of MIM-based PU organogels exhibiting corresponding orange (603 nm, before shuttling or free doping) and blue (451 nm, after shuttling) emissions of the suspended DPAC stoppers as crucial in situ molecular shuttling sensors can be created by force-induced shuttling motions to constrain intramolecular vibrations of DPAC termini. Notably, the brilliant adhesive and self-healing performances together with excellent storage stabilities of MIM-based PU organogels can be verified to provide special force- and temperature-triggered fluorescence emission switches, designating prospective mechano-fluorescence and temperature sensor applications of multi-functional DPAC-based PU organogels in constructing state-of-the-art materials with multi-stimuli responsiveness.

1. Introduction

Together with the swift growth of supramolecular chemistry and materials, many efforts have been devoted to designs and fabrications of mechanically interlocked molecules (MIMs), which are appraised as preeminent platforms to develop artificial molecular machines and stimuli-responsive materials owing to their captivating structures and dynamic natures.[1-4] Rotaxanes, a typical kind of MIMs, are composed of slidable macrocycles threaded onto dumbbell-shaped axle components containing two station reciprocating modes, wherein macrocycles are capable of shuttling back and forth along axle components, and confined by bulky terminated moieties to avoid the detachments of wheel components.[5-9] Moreover, bistable [c2] daisy chain rotaxanes as double-threaded rotaxanes, a specific type of MIMs, comprise two mutually intertwined rotaxane molecules, in which chain-like components of one rotaxane molecule are encircled by slidable macrocycles of the second one through host-guest complexations and vice versa.[10-16] The chain-like axles of interlocked daisy chain

T. T. K. Cuc, Y.-C. Lai, T. M. Khang, H.-C. Lin Department of Materials Science and Engineering Center for Emergent Functional Matter Science National Yang Ming Chiao Tung University Hsinchu 300093, Taiwan E-mail: linhc@nycu.edu.tw



The ORCID identification number(s) for the author(s) of this article can be found under https://doi.org/10.1002/adfm.202519737

© 2025 The Author(s). Advanced Functional Materials published by Wiley-VCH GmbH. This is an open access article under the terms of the Creative Commons Attribution License, which permits use, distribution and reproduction in any medium, provided the original work is properly cited.

DOI: 10.1002/adfm.202519737

W.-T. Chuang National Synchrotron Radiation Research Center Hsinchu 300092, Taiwan

T.-K. W

Department of Biological Science and Technology Center for Emergent Functional Matter Science National Yang Ming Chiao Tung University Hsinchu 300093, Taiwan

R. Rotomskis, S. Steponkiene Biomedical Physics Laboratory National Cancer Institute Vilnius LT-08406, Lithuania



www.afm-journal.de

structures can be decorated with two or more well-defined recognition sites for the macrocycles, resulting in stimuli-driven internal muscle-like motions to donate contracted and extended conformations of bistable [c2] daisy chain rotaxanes. Consequently, the incorporations of functionalized MIMs containing dynamic slide-ring motions into polymeric skeletons to generate mechanically interlocked polymers with stimuli-responsive behaviors have exposed innumerable prospects to be applied in many cutting-edge fields since the existences of mechanical bonds facilitate multiple degrees of molecular motions within polymer architectures. [17–29]

To date, mechanochromic materials in response to external mechanical forces with optical appearance alterations are attracting in materials science, which can be prepared by the integrations of mechanophores with polymeric frameworks to possess molecular conjugation changes by force-induced bond scission or isomerization processes, along with regulations of molecular conformations and intermolecular stacking arrangements upon the exertions of external forces.[30-39] Particularly, radical-based mechanophores, including tetraarylsuccinonitrile, diarylbibenzofuranone, difluorenylsuccinonitrile, etc., comprise dynamic C-C bonds linking two chromic units that undergo reversibly homolytic cleavages (i.e., force-induced bond scissions) and recombined reactions by applying and removing external forces, resulting in relatively stable radical formations along with optical signal variations.[32,33] Isomerization-based mechanophores, such as spiropyran, naphthopyran, rhodamine derivatives, etc., are composed of spiro-junctions that encounter reversible ringopening and ring-closure processes upon respective loading and unloading of mechanical forces (or ultrasonications), bringing about the changes of their optical properties. [32,34-36] Moreover, a variety of organic mechanochromic materials have been established based on stimuli-induced transitions between diverse conformations or molecular packing styles.[37-39]

Notably, polyurethanes (PUs) revealing prominent mechanical properties, shape-memory capabilities, biocompatibilities, etc., bring about considerable developments in constructing various stimuli-responsive PUs with multiple functionalities for many fields of demanding applications. [40-42] As a result, synthetic PUs are commonly exploited scaffolds to invent diverse high-performance mechanochromic polymers as well as highly stretchable and self-healable materials through rational and delicate molecular designs.[43-47] Taking advantage of the force-caused dynamic shuttling behaviors of threaded molecular structures, MIM-based rotaxanes comprising quencherfluorophore pairs as mechanochromic fluorescence force transducers to be imbedded in PU platforms to form rotaxane-based mechanochromic polymers have been announced recently.[48-51] Remarkably, some recent researches focus on the constructions of slide-ring structures of polyrotaxanes and daisy chain molecules to be covalently installed in mechanofluorophoreloaded PU scaffolds to yield MIM-based PU films with ratiometric fluorescence responses toward external mechanical

R. Rotomskis Biophotonics Group, Laser Research Center Physics Faculty Vilnius University Vilnius LT-10222, Lithuania forces.^[52–54] Moreover, by adding quite small amounts of MIMs with slide-ring motions in PU backbones, inherent stretchabilities and toughnesses of aimed PU elastomers could be noticeably amplified.

So far, self-healing polymers can be partially or fully healed to restore initial functionalities autonomously or by extra heating and solvation treatments after their physical damages, which have appeared as a pioneering topic to prolong the longevities of materials and devices, reduce overall costs, and improve sustainable technologies.^[55–59] Accordingly, several efficient strategies for producing self-healing polymers, which can be probably applied to modern technologies, i.e., soft robots, energy storage devices, electronic skins, flexible devices, wearable sensors, protective coatings, etc., are introduced by dynamic covalent bonds, hydrogen bonds, host-guest complexations, metal-ligand co-ordinations, ionic interactions, and so forth. For instance, cellulose nanocrystals (CNCs) can assist self-healing properties of polymeric materials due to their plentiful hydroxyl groups on the surfaces to form multiple hydrogen bonds for creating physical crosslinks in their polymer networks.^[59] Specifically, the unifications of mechanochromic polymers with self-healing functionalities are attractive to fabricate self-healable mechanochromic materials possessing fascinated stimuli-responsive behaviors, adaptabilities, longevities, etc.[60-63] Additionally, polymer gels are regarded as an interesting category of functional soft materials with distinctive features, which are consisted of physically or covalently cross-linked polymer networks swollen in liquid phases.[64,65] Until now, numerous crucial kinds of polymer gels with stimuli-respondent properties, such as organogels, hydrogels, ionogels, organohydrogels, etc., have been explored in different practical applications. Significantly, covalent insertions of mechanophores into polymer gel structures enable to generate mechano-responsive polymer gels with force-induced changes of optical behaviors, which have been demonstrated as ideal platforms to be utilized in the applications of camouflaging, stress/strain sensing, information encoding, and others. [66,67] Consequently, self-healing polymer gels have been created as prospective soft materials because of their excellent reliabilities and long-term stabilities. The reversible chemical or physical cross-linking interactions are responsible for self-healing mechanisms to produce self-healable gel systems with intriguing characteristics.[68,69]

Stimuli-responsive materials have acquired myriad attention on account of their brilliant applications in sensor, anticounterfeiting, data storage, molecular switch, electronic skin materials, and others.[70-73] These intelligent materials reveal the alterations of their physical or/and chemical characteristics responding to certain external stimulations, i.e., chemical reagents, temperatures, light irradiations, forces, electric fields, magnetic fields, etc. In particular, organic luminescent materials with rapid and efficient reactions toward diverse environmental stimuli to offer obvious variations in their optical properties are really essential both in basic sciences and technique applications.[74-83] Importantly, various conformation-adaptive fluorophores derived from 9,14diphenyl-9,14-dihydrodibenzo[a,c]phenazine (DPAC) derivatives with unique vibration-induced emission (VIE) effects have been exploited in optical displays, dynamic emissive materials, and so on.^[84-88] Interestingly, VIE-active moieties with bi-stable



www.afm-journal.de

states display long-wavelength/orange-red fluorescence emissions in their unconstrained states (planar states), whereas short-wavelength/blue fluorescence emissions can be observed in constrained states (bent states). By virtue of notably structural and/or configurational changes in excited states, the ratios of short- and long-wavelength bands along with dual fluorescence emission responses of VIE-active fluorogens can be readily tuned by modulating intramolecular vibrations through the fluctuations of temperatures, viscosities, etc., providing extraordinary multi-colors of these fluorescence materials. [89–94]

Recently, new VIE-active [2]rotaxanes have been prepared via the combinations of [2]rotaxane structures with representative DPAC moieties as bulky stoppers. [95] More essentially, these obtained [2]rotaxanes exhibited tunable VIE properties and switchable circularly polarized luminescence features due to their dual stimuli-responsive behaviors toward both solvent and anion as external stimuli to induce reversible molecular motions of chiral wheels in [2]rotaxane structures. Accordingly, the VIE-based [2]rotaxanes demonstrated orange-red emissions initially with more freedom of the DPAC stopper and then displayed blue emissions after shuttling upon adding either the solvent (ethylene glycol) or anion (CF₃COO⁻) due to the increased constraints of the DPAC moiety. In addition, a series of DPAC moieties have been introduced into PU films by diverse physical blending or chemical bonding (as main-chain backbone and side-chain pendants) to show their characteristic PL emission colors as temperature sensors, which could be assigned to different constraints of DPAC moieties via different physical doping and chemical bonding confinements along with temperature responses in polymer films.[96] Furthermore, two DPAC derivatives with special VIE behaviors have been synthesized to be simply doped into poly(εcaprolactone) and ethylene vinyl acetate systems to achieve blend films possessing continuous PL emission color changes (only from pink to blue emissions) upon stretching and temperature variations based on successive alterations of conformation and confinement for DPAC molecules.[97] Hence, the approaches of DPAC-based mechano-fluorescent materials in polymer gel systems with the benefits of enormous ratiometric emission contrasts and extra self-healabilities are of great interests, because the more free forms of DPAC units exhibiting orange emissions in the gel state initially will be transformed into their highly constrained forms to reveal blue emissions (with huge fluorescence color changes) upon external forces.

Aiming at the designs and fabrications of self-healable PU organogels possessing novel mechano-fluorescent properties, the DPAC units as stoppers with appealing vibration-induced emission features have been integrated into the artificial molecular muscle structures of MIMs, i.e., [2]rotaxanes and [c2] daisy chain molecules. In contrast to traditional daisy chain molecules with the axle-exerted force mode, which have been described in our previous report, [53] unconventional daisy chain rotaxanes with another macrocycle-exerted force mode are developed in this study. These unconventional daisy chains can be grafted with polymer backbones through macrocyclic components rather than via stopper moieties of normally reported daisy chain molecules, to avoid the restrictions of intramolecular motions of DPAC stoppers with double linkages attached to polymer matrices in traditional daisy chain molecules. As a consequence, the newly designed [2]rotaxanes and daisy chains consisting of VIE-active

DPAC stoppers are inserted into PU skeletons to acquire corresponding self-healable PU organogels, which would render ratiometric fluorescence changes by external mechanical forces, i.e., an orange emission ($\lambda_{\rm em}$ = 603 nm) in the unconstrained state (before stretching) and a blue emission ($\lambda_{em} = 451$ nm) in the condensed state (after stretching), due to the dynamic sliding motions of DPAC stoppers with respect to the macrocyclic movement by exerted forces to induce more restricted intramolecular vibrations of DPAC units and thus to display blue shifted emissions. Furthermore, the shuttling processes of macrocycles and DPAC stoppers in [2]rotaxanes and daisy chain molecules can be modulated upon chemical stimulations to yield divergent confinements of DPAC units accompanied by the corresponding optical and mechanical properties in their respective PU organogels. It is important that amide groups in PU frameworks can support self-healing properties, thus cellulose nanocrystals (CNCs) are incorporated into PU organogel systems to generate hydrogen bonding interactions, facilitating effective self-healing characteristics of PU organogels. Also, CNCs can dissipate energy to improve stretchable capabilities and toughnesses of the obtained PU organogels. Furthermore, the distinctive adhesion features of targeted PU organogels on different substrates can be provided to further verify their prospective applications in developing stimuli-responsive smart materials.

2. Results and Discussion

2.1. Molecular Design and Synthesis

As stated by our previous publication,^[53] as shown in Schemes S2 and S3, targeted DPAC-based [2]rotaxanes RDPAC/1 and RDPAC/2 (before and after shuttling, respectively) along with corresponding extended/contracted [c2] daisy chain molecules with macrocycle-exerted force modes DDPAC/E and DDPAC/C were produced through the self-sorting strategies of macrocyclic component-based electron-rich DB24C8 cavities and linear axle-based electron-poor secondary ammonium moieties via strong electrostatic host-guest interactions. Afterwards, the respective intermediate [2]rotaxane 11 and [c2] daisy chain 13 consisting of original dibenzylammonium (DBA) binding stations were gained by using the Cu(I)-catalyzed Huisgen alkyneazide 1,3-dipolar cycloaddition (CuAAC) reactions as the classic end-capping reactions between pseudo-[2]rotaxane 10 and pseudo-[c2] daisy chain 12 with the DPAC-based terminated group DPAC-OC₃H₃ under mild conditions. Subsequently, the N-methyltriazolium (MTA) units as the other selective recognition sites of [2]rotaxanes and [c2] daisy chain molecules were offered through the methylations of triazole moieties on compounds 11 and 13 with iodomethane together with the ionexchange processes by utilizing the oversupply of saturated NH₄PF₆ solution to produce [2]rotaxane RDPAC/1 (before shuttling) and bistable [c2] daisy chain DDPAC/C in its contracted conformation decorated with two types of binding sites at different positions (see Schemes S2 and S3), in which DB24C8 cavities were located in DBA sites initially. In addition, the molecular shuttling motions of DB24C8 wheels from DBA to MTA binding sites to provide [2]rotaxane

RDPAC/2 (after shuttling) and [c2] daisy chain molecule DDPAC/E in the expanded form would be achieved by



www.afm-journal.de

neutralizing DBA stations in the corresponding [2]rotaxane RD-PAC/1 and [c2] daisy chain molecule DDPAC/C before shuttling (see Schemes S2 and S3 along with Figure 1). Accordingly, it was proposed that MIM structures of [2]rotaxanes and [c2] daisy chain molecules displayed efficiently reversible molecular reciprocating motions of RDPAC/1 and DDPAC/C along with RDPAC/2 and DDPAC/E conformations owing to sliding movements of DB24C8 wheels between two distinct recognition sites toward external chemical stimuli (see Figure 1).

Since both MIM structures of [2]rotaxanes and [c2] daisy chain molecules (before and after shuttling) all possessed blue PL emissions in solid state, the solutions of these MIMs need to be investigated. Thus, the impacts of mixed solutions on optical properties of both [2]rotaxane RDPAC/1 and daisy chain molecule DDPAC/C should be considered because of their distinct ratiometric emission colors in different solvents. Both solvents of anisole and DMSO were utilized in subsequent illustrations of mechano-fluorescent polymer organogels owing to their high boiling temperatures to maintain their stable gel state after certain storage periods and good bio-compatibilities. As shown in Figure S1 (Supporting Information), the orange emission bands (at 603 nm) of RDPAC/1 and DDPAC/C were shifted to the blue bands (at 451 nm) as the volume fractions of DMSO were increased in the mixed solvents of anisole/DMSO due to the higher polarity and viscosity of DMSO. Thus, the mixed solvent of anisole/DMSO (75/25, v/v), in which the orange emissions of both RDPAC/1 and DDPAC/C were quite prominent, was selected as a green solvent mixture to be used in selfhealable organogel systems because anisole could not totally dissolve mechano-fluorescent polymers alone in this study. As a result, the dissimilar PL behaviors for [2] rotaxanes RDPAC/1 and RDPAC/2 along with daisy chain molecules DDPAC/C and DDPAC/E in the mixed solutions of anisole/DMSO (75/25, v/v) could be demonstrated in Figure 1e,f, where both RDPAC/1 and **DDPAC/C** solutions emitted orange fluorescence colors initially in contrast to blue fluorescence emissions observed in both neutralized RDPAC/2 and DDPAC/E solutions (after shuttling) by adding base due to the higher restraints of their DPAC stoppers. These phenomena were consistent with the expectations for final demonstrations of DPAC-based MIMs integrated into PUbased organogel systems to reveal various ratiometric mechanofluorescence emissions during stretching processes. Moreover, the aggregation features of DPAC moieties in both RDPAC/1 and DDPAC/C could be examined in THF/H2O semi-aqueous solutions with different water fractions. As presented in Figure S3 (Supporting Information), by increasing water contents from 0 to 95%, the blue emission intensities of RDPAC/1 and DDPAC/C were augmented simultaneously, proposing the enhanced confinements of DPAC moieties in THF/H2O semi-aqueous solutions by adding water. Accordingly, the DPAC-based MIMs incorporated into PU-based solid films all remained blue PL emissions before and after stretching (as shown in Figure S4, Supporting Information) owing to the highly aggregated restraints of their DPAC units in solid state, which could not illustrate obvious mechano-fluorescence behaviors, so the rational designs of PU-based organogels in 80 wt.% of the mixed anisole/DMSO (75/25, v/v) solvent featuring ratiometric emissions become required in this study. As provided in Figure \$5 (Supporting Information), the schematic illustrations for distinct microenvironments of DPAC moieties within PU-based solid films versus organogels clarified the contributions of different environments to DPAC moieties with respective blue and orange PL emissions witnessed in their solid and organogel forms. Consequently, bistable [2]rotaxanes RDPAC/1 and RDPAC/2 (before and after shuttling) along with extended/contracted [c2] daisy chain molecules DDPAC/E and DDPAC/C were covalently integrated into PU frames to create PU-CNC-RDPAC/1, PU-CNC-RDPAC/2, PU-CNC-DDPAC/E, and PU-CNC-DDPAC/C polymeric organogels, respectively. It could be hypothesized that bistable [2]rotaxanes and [c2] daisy chain molecules containing fluorophoric DPAC stoppers acted as stimuli-responsive fluorescence molecules would reveal divergent optical and mechanical responses in PU organogel systems under external tensile forces, which could be assigned to their distinct molecular structural characteristics. In these designed [2]rotaxanes and daisy chain molecules, the tensile force-activated sliding motions of DB24C8 wheels along their linear axle components could directly adjust the distances between DB24C8 wheels and fluorophoric DPAC moieties in PU organogels, and thus to regulate fluorescence emission colors of DPAC units by manipulating their constrained conformations. Accordingly, these MIM moieties in PU-CNC-RDPAC/1 and PU-CNC-DDPAC/C organogels would feature conspicuous sliding movements and exhibit orange emissions of DPAC units initially as shown in Figure 2a, which may further encounter tightened conformations to show distinct PL emission color changes upon stretching as excellent mechano-fluorescent PU organogels. However, [2]rotaxane and daisy chain moieties in PU-CNC-RDPAC/2 and PU-CNC-DDPAC/E organogels would almost entirely tighten their compact conformations to suffer constrained shuttling motions and display blue emissions of DPAC units (even without any stress).

As shown in Figure 2b, the synthetic pathways of designed force-induced tunable fluorescence switching behaviors of PU organogels incorporating various VIE-active DPAC-based [2]rotaxanes and extended/contracted [c2] daisy chains are described, where mechano-responsive PU organogels consisted of different amounts of hexamethylene diisocyanate (HDI), isophorone diisocyanate (IPDI), tetra-ethylene glycol (TEG), cellulose nanocrystals (CNCs), and DPAC-based MIM units (i.e., [2]rotaxanes and [c2] daisy chains). The whole synthetic procedures and related chemical characterizations of all intermediates and targeted compounds are provided in the Supporting

Information. The step-growth polymerizations were employed to construct mechano-sensitive PU organogels containing DPAC-based MIMs, wherein HDI and IPDI monomers, TEG chain extender, CNCs cross-linker, DPAC mechano-responsive fluorophore, and diverse shuttling motions of MIMs as artificial molecular muscles were catalyzed by dibutyltin dilaurate (DBTDL). Besides, the stoichiometric ratios of reactive groups were managed to warrant plausible complete reactions between -OH and -NCO groups, which could emerge effortlessly to create amide units in polymeric organogels. On the other hand, a standard sample **PU-CNC** without DPAC-modified MIM structures implanted in the polymer network was also supplied as a model derivative to be compared in this study.

16163028, 0, Downloaded from https://advanced.onlinelibrary.wiley.com/doi/10.1002/adfm.202519737 by Vilnius University, Wiley Online Library on [22/10/2023]. See the Terms and Conditions (https://onlinelibrary.wiley.

and-conditions) on Wiley Online Library for rules of use; OA articles are governed by the applicable Creative Commons License

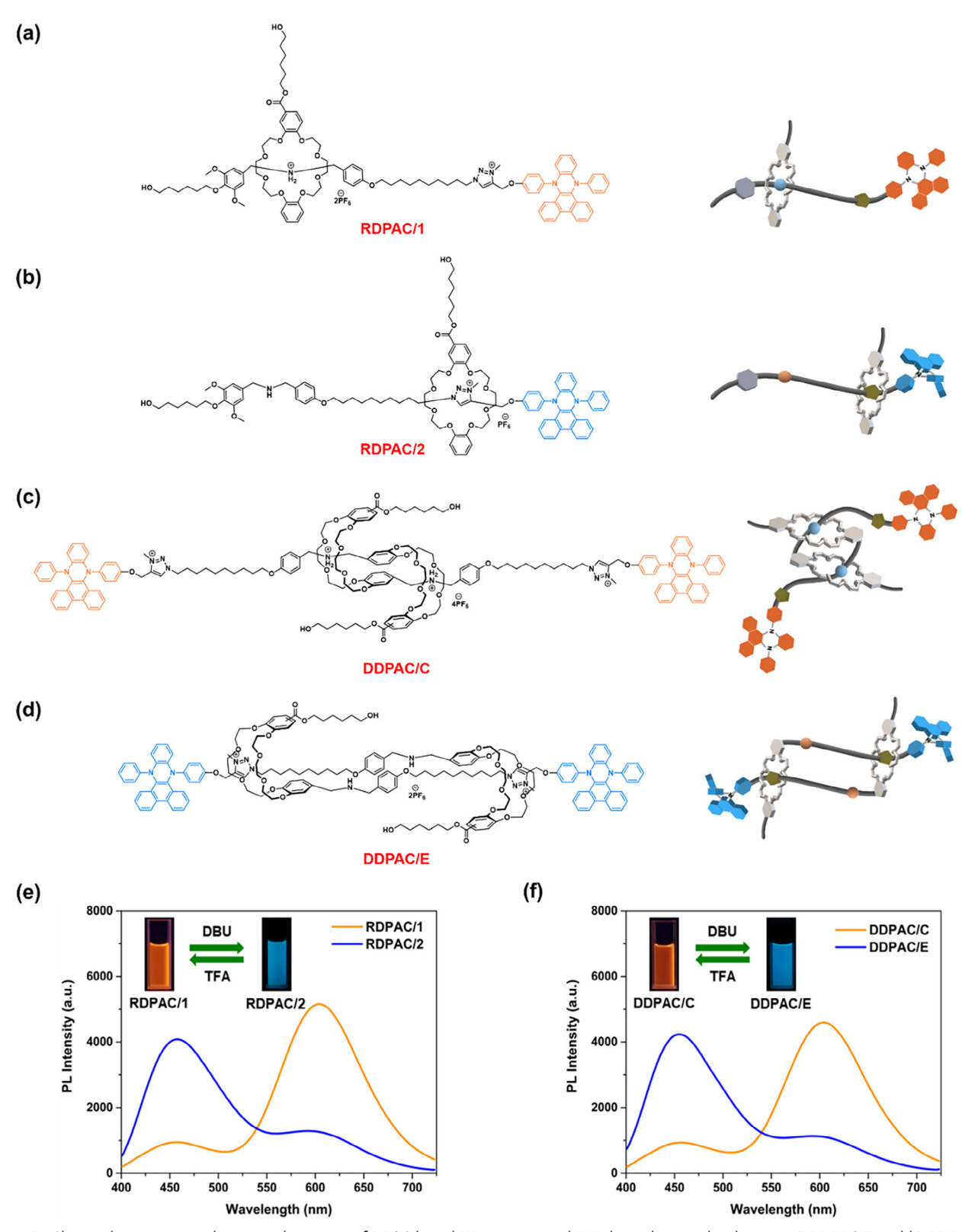


Figure 1. Chemical structures and cartoon depictions of DPAC-based [2]rotaxanes and [c2] daisy chain molecules, i.e., a) RDPAC/1 and b) RDPAC/2 (before and after shuttling, respectively) along with c) DDPAC/C and d) DDPAC/E (contracted and expanded forms, respectively). PL spectra of e) [2]rotaxane RDPAC/1 and f) [c2] daisy chain DDPAC/C (orange lines before shuttling) in anisole/DMSO (75/25, v/v) solutions were neutralized by adding base (DBU) to become respective solutions of [2] rotaxane RDPAC/2 and [c2] daisy chain DDPAC/E (blue lines after shuttling), where the inset figures show their PL emission colors and acid-base responses (Concentration: 0.2 mg mL⁻¹, $\lambda_{ex} = 365$ nm).

16163028, 0, Downloaded from https://advanced.onlinelibrary.wiley.com/doi/10.1002/adfm.202519737 by Vilnius University, Wiley Online Library on [22/10/2023]. See the Terms and Conditions (https://onlinelibrary.wiley.

and-conditions) on Wiley Online Library for rules of use; OA articles are governed by the applicable Creative Commons License

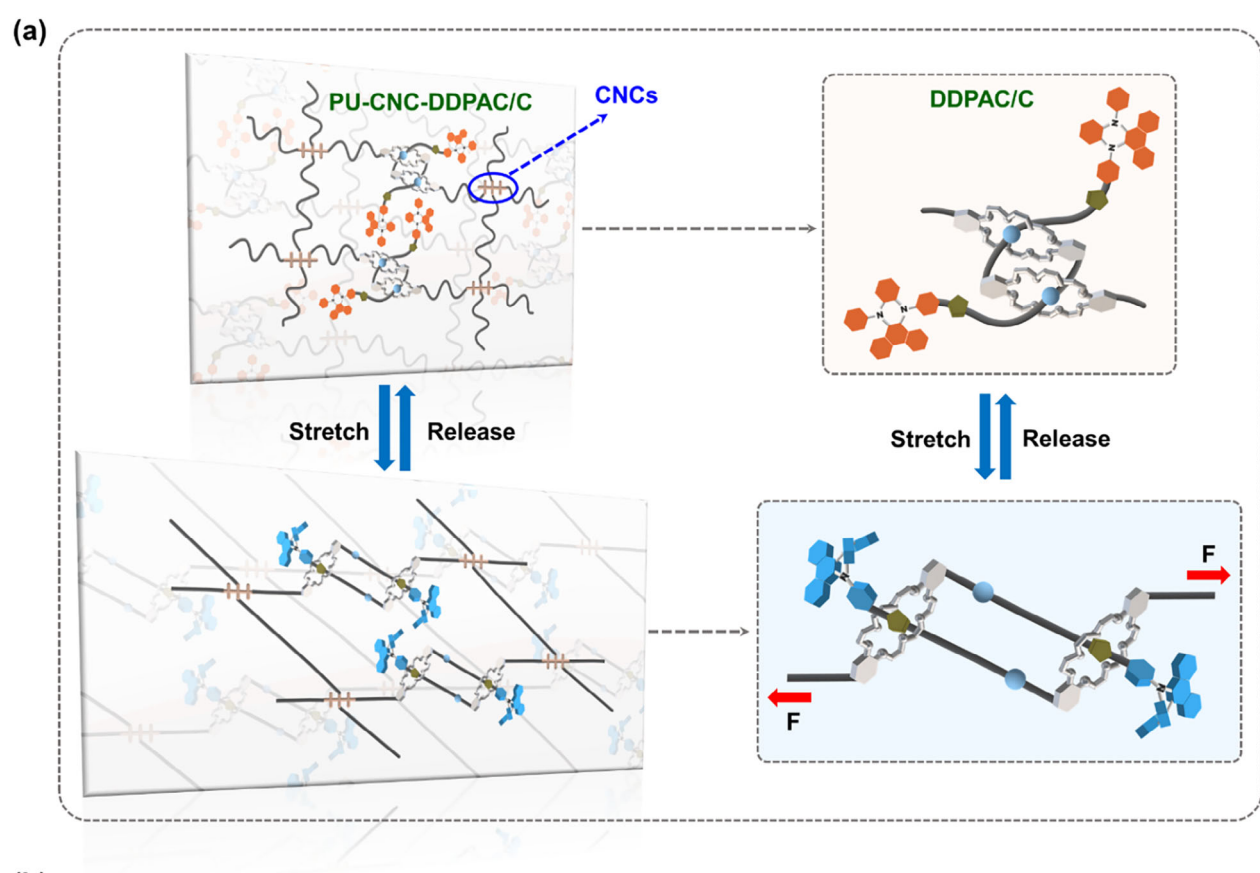


Figure 2. a) Cartoon representations of force-induced slide-ring motions to regulate ratiometric fluorescence emission switching for PU-CNC-DDPAC/C organogel. b) Synthetic routes and chemical structures of mechano-fluorescent PU organogels containing DPAC-based MIMs, including [2] rotaxanes RDPAC/1 and RDPAC/2 (before and after shuttling) along with [c2] daisy chains DDPAC/C and DDPAC/E (contracted and expanded forms).





www.afm-journal.de

2.2. Chemical and Thermal Characterizations of PU Organogels

Fourier-transform infrared spectroscopy (FTIR) measurements were proceeded for the investigation of the simple reaction between -NCO (in HDI and IPDI) and -OH groups (in TEG and CNCs) to form amide units in the standard sample PU-CNC (without MIMs) via poly-condensation reactions (see Figure 2b). As shown in Figure S6a (Supporting Information), the stretching vibration of -OH groups in TEG and CNCs could be detected ≈3300 cm⁻¹, and the distinctive band at 2250 cm⁻¹ related to -NCO groups in HDI and IPDI could also be discerned. Nonetheless, after polymerization the wide-range band ca. 3300 cm⁻¹ became narrowed, the characteristic band at 2250 cm⁻¹ diminished, the N-H stretching vibration emerged at 3300 cm⁻¹ along with amide I and II bands at 1700 and 1550 cm⁻¹, identifying the complete reaction of -NCO and -OH groups effectively. Furthermore, the thermal properties of PU organogels could be surveyed by thermo-gravimetric analysis (TGA) as shown in Figure S6b (Supporting Information), where TGA curves exposed high thermal stabilities of PU organogels.

2.3. Mechanical Properties of PU Organogels

The excellent mechanical strengths as well as outstanding stretchable capabilities were realized as the most essential issues of PU organogels for their practicable applications in stretchable mechano-fluorophoric sensors to differentiate the variations of ratiometric emissions upon tensile forces. Hence, various feed molar ratios of the monomer components were compiled and presented in Table S1 (Supporting Information) to ascertain optimal stoichiometric proportions for the productions of PU organogels based on their mechanical properties. As shown in Figure \$7a (Supporting Information), the amount of CNCs cross-linker (as a reinforcing agent) was fixed at 0.5 wt.% initially, and the ideal molar ratio of IPDI and HDI was found to be 75:25, which could be used to prepare a standard PU-CNC organogel as the most basic organogel sample, because the intensified molar ratio between IPDI and HDI from 75:25 to 100:0 in PU-CNC-4 organogel deteriorated the PU organogel with decreased toughness and stretchability in contrast to the standard PU-CNC organogel. In addition, as shown in Figure \$7b (Supporting Information), the optimum amount of 0.5 wt.% CNCs cross-linker in PU-CNC organogel was further verified to possess the highest toughness of 54.97 MJ m⁻³ (with a tensile stress of 2.20 MPa and a tensile strain ca. 2943% see Table S1, Supporting Information) in comparison with some analogous organogels containing less contents of CNCs (i.e., 0 and 0.25 wt.% in corresponding PU-CNC-5 and PU-CNC-6) as well as higher amounts of CNCs (i.e., 0.75 and 1.0 wt.% in respective PU-CNC-7 and PU-CNC-8) disclosed worse mechanical properties. Consequently, the molar ratio of IPDI and HDI was fixed at 75:25 (2.0 mmol and 0.67 mmol) with 0.5 wt.% CNCs cross-linker as the standard recipe of PU-CNC organogel, which was further utilized to examine enriched mechanical toughnesses along with force-triggered slide-ring motions to reveal ratiometric fluorescence switching behaviors initiated by the introductions of DPAC-based MIM structures into PU skele-

Adv. Funct. Mater. 2025, e19737

tons (i.e., [2]rotaxanes RDPAC/1 and RDPAC/2 along with [c2] daisy chains DDPAC/C and DDPAC/E before and after shuttling, respectively). Importantly, different strain rates of 10, 20, and 30 mm s⁻¹ were employed to investigate their effects on mechanical features of the standard PU-CNC organogel as demonstrated in Figure S7c,d (Supporting Information), wherein the shorter tensile strains were achieved with the faster strain rates. Thereby, the highest strain rate of 30 mm s⁻¹ in comparison with 1 mm s⁻¹ of our previous publications^[52–54] was selected to gain the shortest tensile strain, which would be appropriate for the further enhancements of marvelous strains upon the integrations of various MIMs as artificial molecular muscles into PU frameworks.

Subsequently, different sliding motion effects of DPACfunctionalized MIMs (i.e., [2]rotaxanes RDPAC/1 and RDPAC/2 as well as [c2] daisy chains DDPAC/C and DDPAC/E) on the mechanical properties of MIM-based PU organogels were also explored. Therefore, a number of mechano-fluorophoric PU organogels containing various amounts of MIM components with distinctive mechanical behaviors are provided in Tables S2 and S3 and Figure S8 (Supporting Information) (i.e., stressstrain curves of related PU organogels with a strain rate of 30 mm s⁻¹). As proven in Figure S8 (Supporting Information), the progressively enhanced toughnesses with the superior stretchabilities (tensile strains) could be detected by magnifying amounts of [2]rotaxanes and [c2] daisy chain units from 0 to 1.5 wt.%, which might be attributed to dynamic sliding motions of MIMs with enhanced energy dissipation capacities to offer greater elongations. However, the optimum tensile strains and toughnesses of PU-CNC-RDPAC/1 and PU-CNC-DDPAC/C organogels (containing 1.5 wt.% of [2]rotaxanes and [c2] daisy chain units) were slightly dropped by introducing MIM components over 1.5 wt.% due to more complex structural arrangements and aggregations of MIMs (see Figure S8 and Tables S2 and S3, Supporting Information). Attractively, benefiting from varied sliding motions of DPAC-based MIMs, PU-CNC-RDPAC/1 and PU-CNC-DDPAC/C organogels demonstrated evidently superior mechanical properties, including stretchabilities and toughnesses, than their comparable PU-CNC-RDPAC/2 and PU-CNC- DDPAC/E organogels in Figure 3, wherein [2]rotaxane RDPAC/1 and [c2] daisy chain DDPAC/C (before shuttling) possessed longer gliding distances than their counterparts RDPAC/2 and DDPAC/E (after shuttling) proven by their ratiometric PL emissions (orange/blue colors) of DPAC stoppers with different constraints (free/restricted conformations) as illustrated in Figure 1e,f. According to the structural features of MIMs, both [2]rotaxane RDPAC/1 and [c2] daisy chain DDPAC/C (before shuttling) in polymeric materials owned obvious long-range sliding distances accompanied by releasing hidden alkyl chains between DB24C8 rings to accumulate numerous microscopic motions, leading to toughened mechanical properties of corresponding materials. On the other hand, both [2]rotaxane RDPAC/2 and [c2] daisy chain DDPAC/E (after shuttling) in polymer matrices mostly tighten their compact conformations along with constrained sliding motions, to illustrate the correlation between their extents of sliding motions and increased toughnesses. These results suggested the significant impacts of MIMs on the advanced features of inherent mechanical properties for these perfectly

www.afm-journal.de

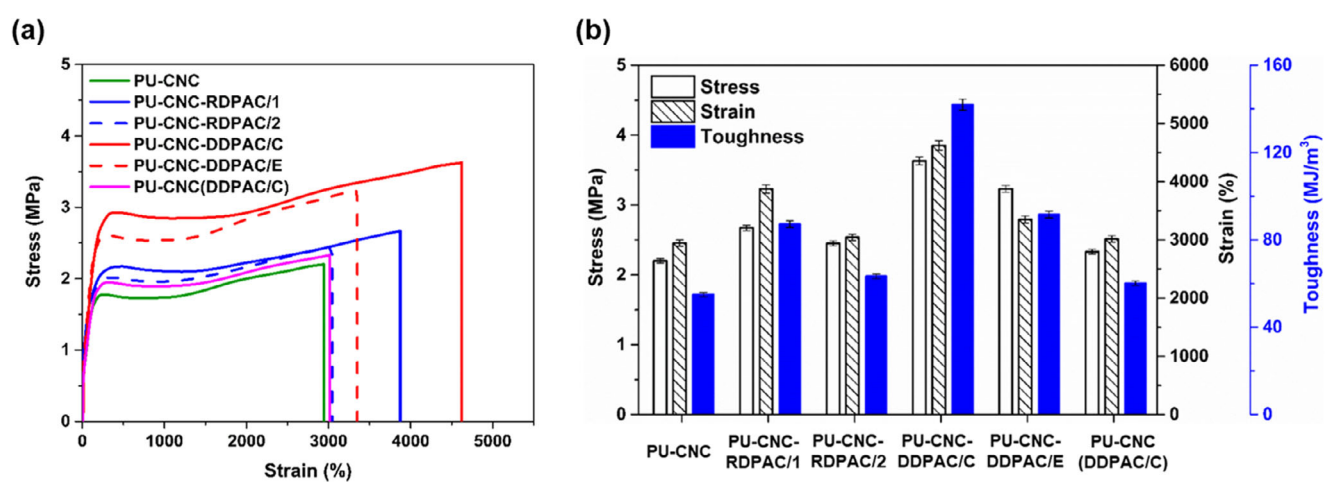


Figure 3. a) Stress–strain curves and b) stress/strain/toughness histograms of the standard **PU-CNC** (without MIMs) organogel along with MIMbased organogels, i.e., **PU-CNC-RDPAC/1**, **PU-CNC-RDPAC/2**, **PU-CNC-DDPAC/C**, and **PU-CNC-DDPAC/E** containing DPAC-based MIMs (1.5 wt.%), including [2]rotaxanes **RDPAC/1** and **RDPAC/2** (before and after shuttling) as well as [c2] daisy chains **DDPAC/C** and **DDPAC/E** (contracted and expanded forms) accompanied by the blended **PU-CNC(DDPAC/C)** organogel containing 1.5 wt.% of freely doped [c2] daisy chain **DDPAC/C**, which was physically blended into the standard **PU-CNC** organogel (at a strain rate of 30 mm s⁻¹).

designed mechano-fluorescent PU organogels. Prominently, PU-CNC-DDPAC/C organogel exhibited the highest toughness and stretchability (i.e., strain) in contrast to PU-CNC-RDPAC/1 organogel (see Figure 3 and Table 1), which might be ascribed to the artificial molecular structure of [c2] daisy chain DDPAC/C as double-threaded rotaxanes holding less entanglements of dangling DPAC stoppers through efficient sliding processes compared with those of [2]rotaxane RDPAC/1. Certainly, the integrated PU-CNC-RDPAC/1+DDPAC/C organogel comprising both [2]rotaxane RDPAC/1 and [c2] daisy chain DDPAC/C (0.75 wt.% of both MIMs, i.e., 1.5 wt.% of total MIMs) revealed the medium toughness and stretchability in comparison with PU-CNC-DDPAC/C and PU-CNC-RDPAC/1 organogels (see Table S5, Supporting Information). Importantly, the blended PU-CNC(DDPAC/C) organogel consisting of [c2] daisy chain DDPAC/C (1.5 wt.%) physically blended into the standard PU-CNC organogel also exhibited a worse stretchable capability and a lower toughness in contrast to the optimal PU-CNC-DDPAC/C organogel as proven in Figure 3 and Table 1, which could be assigned to no covalently linked contributions of slidable motions from artificial molecular

muscles (i.e., MIMs) to promote mechanical behaviors of prepared organogels. Originated from the mechanical properties of all MIM-based PU organogels, the toughnesses of PU organogels could be estimated and shown in Figure 3b and Table 1, whereas PU-CNC-RDPAC/1 organogel also unveiled an improved toughness of ≈87 MJ m⁻³ and a strain of 3874%, which were ca. 1.6 times higher toughness and 1.3 times larger strain than those of \approx 55 MJ m⁻³ and 2943% belonged to the standard PU-CNC organogel (without MIMs). In the meantime, PU-CNC-DDPAC/C organogel exhibited a superior toughness of \approx 142 MJ m⁻³ and a strain of 4623% which had ≈2.6 times higher toughness and 1.6 times larger strain in comparison to PU-CNC organogel (without MIMs), confirming the crucial artificial molecular muscle task of [c2] daisy chain component (just by integrating ca. 1.5 wt.% of DDPAC/C) in the boosted toughnesses of newly designed PU organogels. As a result, the optimal PU-CNC-DDPAC/C organogel containing 1.5 wt.% of MIMs possessed the best toughness of \approx 142 MJ m⁻³ and the highest strain of 4623% among all of developed DPACbased PU organogels, which could be further inspected in later experiments.

Table 1. Mechanical Properties of PU Organogels Consisting of Different Types of MIMs (Including [2] Rotaxanes and [c2] Daisy Chain Molecules).

PU Samples ^{a)}	Tensile Stress [MPa]	Tensile Strain [%]	Toughness [MJ m ⁻³]
PU-CNC ^{b)}	2.20	2943 ± 54	54.97 ± 1.0
PU-CNC-RDPAC/1 ^{b)}	2.67	3874 ± 72	87.17 ± 1.6
PU-CNC-RDPAC/2 ^{b)}	2.45	3044 ± 58	63.36 ± 1.2
PU-CNC-DDPAC/C ^{b)}	3.63	4623 ± 85	141.92 ± 2.7
PU-CNC-DDPAC/E ^{b)}	3.23	3349 ± 63	91.62 ± 1.7
PU-CNC(DDPAC/C) ^{c)}	2.33	3016 ± 55	60.17 ± 1.1

a) Mechanical tests of PU organogels were proceeded by using a strain rate of 30 mm s⁻¹; b) The standard **PU-CNC** (without MIMs) organogel along with MIM-based organogels, i.e., **PU-CNC-RDPAC/1**, **PU-CNC-RDPAC/2**, **PU-CNC-DDPAC/C**, and **PU-CNC-DDPAC/E** containing DPAC-based MIMs (1.5 wt.%), including [2] rotaxanes **RD-PAC/1** and **RDPAC/2** (before and after shuttling) as well as [c2] daisy chains **DDPAC/C** and **DDPAC/E** (contracted and expanded forms); c) The blended **PU-CNC(DDPAC/C)** organogel containing 1.5 wt.% of freely doped [c2] daisy chain **DDPAC/C** (contracted form), which was physically blended into the standard **PU-CNC** organogel.



www.afm-journal.de

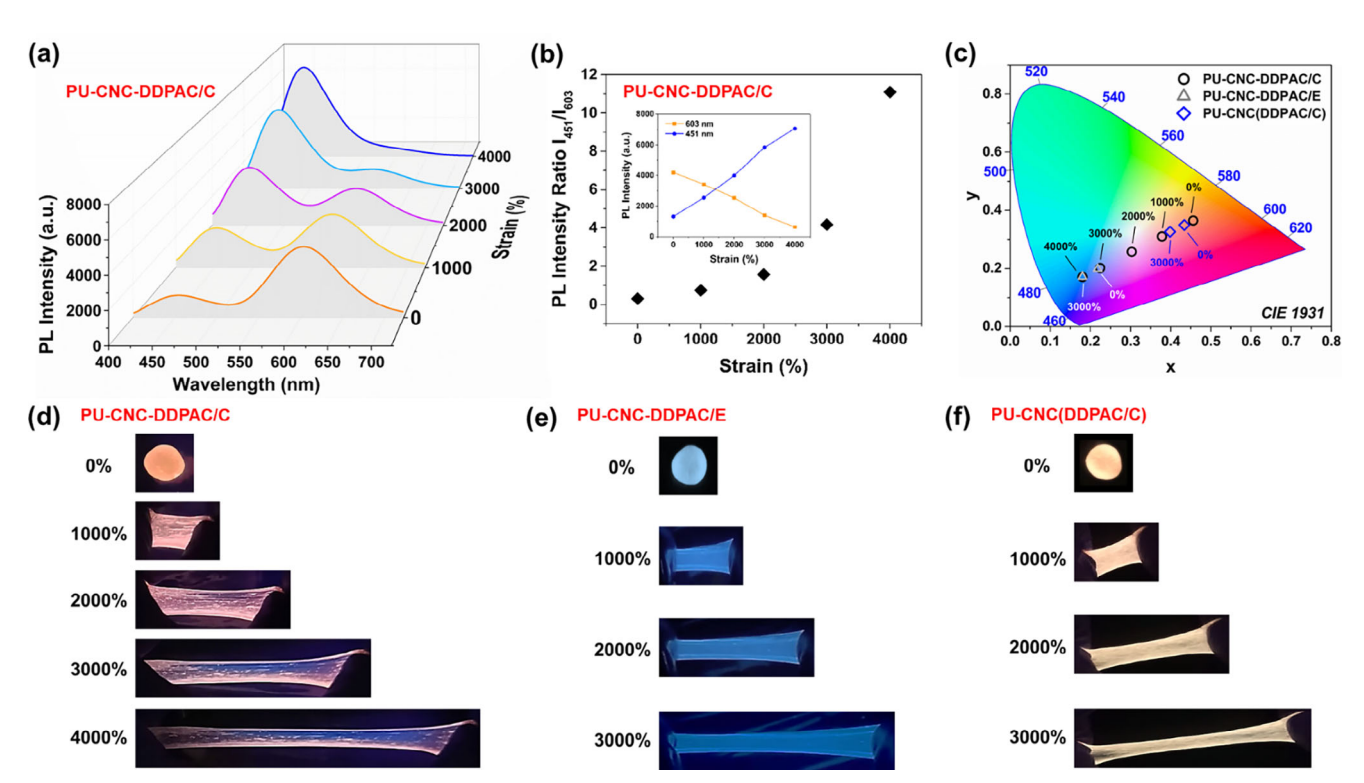


Figure 4. a) PL spectra and b) Plots of PL intensity ratios (I_{451}/I_{603}) between blue ($\lambda_{em}=451$ nm) and orange ($\lambda_{em}=603$ nm) fluorescence emissions for PU-CNC-DDPAC/C organogel with different tensile strains ($\lambda_{ex}=365$ nm). c) CIE 1931 coordinates of PU-CNC-DDPAC/C, PU-CNC-DDPAC/E, and PU-CNC(DDPAC/C) organogels with different tensile strains. Photographs of d) PU-CNC-DDPAC/C organogel (containing MIMs before shuttling), e) PU-CNC-DDPAC/E organogel (containing MIMs after shuttling), and f) blended PU-CNC(DDPAC/C) organogel (containing freely doped MIMs without shuttling) under diverse elongation tests, where images were taken under an UV lamp ($\lambda=365$ nm).

2.4. Ratiometric PL Emissions of PU Organogels as Mechano-Fluorescence and Temperature Sensor Materials

Fundamentally, DPAC derivatives, one kind of advanced ratiometric fluorophores performing exclusive VIE effects, exhibited blue emission colors in the constrained state but revealed orange fluorescence emissions in the free state, experiencing distinctive fluorescence color changes owing to the variations of their intramolecular vibrations. Additionally, the integrations of DPAC-based MIMs ([2]rotaxanes RDPAC/1 and RDPAC/2 along with daisy chains DDPAC/C and DDPAC/E) with diverse shuttling motions (before and after shuttling) to polymer networks were proposed not only to upgrade intrinsic mechanical properties of PU organogels by sliding effects, but also to display dual fluorescence emissions through the VIE behaviors of DPAC stoppers, which could be mechanically tuned by external tensile forces as ratiometric mechano-fluorescence units. The feasible schematic illustration of bistable fluorescence responses from orange to blue emissions upon stress for PU organogels containing DPAC-based [c2] daisy chain molecules was clarified in Figure 2a. The excitation wavelength of λ_{ex} = 365 nm was chosen for all PL measurements of MIM-based PU organogels (similar to the previous PL measurements of DPAC-based MIM solutions) in this study, which was based on the UV-vis spectra of PU-CNC- RDPAC/1 and PU-CNC-DDPAC/C organogels before and after stretching displayed in Figure S9 (Supporting Information). Consequently, the fluorescence emission changes of PU-CNC-DDPAC/C and PU-CNC-RDPAC/1 organogels consisting of DPAC-modified [c2] daisy chain molecule DDPAC/C and [2]rotaxane RDPAC/1 upon stretching were systematically surveyed by PL measurements shown in Figure 4 and Figure \$10 (Supporting Information). Upon stretching, PU-CNC-DDPAC/C and PU-CNC-RDPAC/1 organogels exposed mainly initial orange to final blue fluorescence emissions (at 603 and 451 nm, respectively) associated with the hindrance of intramolecular vibrations in conformationadaptive DPAC fluorophores, because of the mechanical forceinduced shuttling motions of DB24C8 macrocycles to reduce the freedom of DPAC stoppers after shuttling. According to the stress-strain curves of PU organogels in Figure 3a, PU-CNC-DDPAC/C organogel displayed the lengthiest tensile strain to enable the strongest blue fluorescence emission at 451 nm due to the highest degree of conformation transition from planar to bent of DPAC moieties. Moreover, the ratiometric PL emissions of I_{451}/I_{603} (PL intensity ratios of blue and orange colors) for PU-CNC-DDPAC/C organogel versus various strains (0-4000%) were plotted in Figure 4b. Also, the CIE diagrams and photographs of PU-CNC-DDPAC/C and PU-CNC-RDPAC/1 organogels (containing MIMs before shuttling) illustrated distinct PL emission variations from orange to blue colors (covering wide ranges of CIE coordinates) under various tensile strains of 0-4000% and 0-3000% in Figure 4c,d and Figure S10c,d (Supporting Information), respectively. Besides, the mechano-responsive PL emission switching of PU-CNC-DDPAC/C organogel in Figure 4c



DDPAC/C organogel before and after stretching were investigated and shown in Figure 5d,e. The stretched **PU-CNC-DDPAC/C** organogel exhibited a shorter lifetime value of the orange emission at 603 nm ($\tau_{603} = 3.30$ ns after stretching) of DPAC moieties than that of the un-stretched one ($\tau_{603} = 6.07$ ns before stretching), whereas a longer lifetime value of the blue emission at 451 nm ($\tau_{451} = 6.23$ ns after stretching) of DPAC units in the stretched **PU-CNC-DDPAC/C** organogel was yielded in contrast to the pristine organogel ($\tau_{451} = 3.41$ ns before stretching), signifying appealing ratiometric PL responses of DPAC-based MIMs integrated in mechano-responsive PU organogels.

Subsequently, the recoveries of ratiometric PL emissions in the stretched PU-CNC-DDPAC/C organogel at ambient temperature were examined in different time intervals to explore reversible mechano-fluorescence emission switching behaviors. As exhibited in Figure S12a,b (Supporting Information), the blue emission ($\lambda_{\rm em}$ = 451 nm) was reduced gradually and reached an equilibrium state after 3 h at room temperature after removing tensile forces. In the meanwhile, the orange emission ($\lambda_{\rm em} = 603$ nm) could be regained efficiently up to 93.7% after 3 h of restoration. Alternatively, the blue emission of the stretched PU-CNC-DDPAC/C organogel was disappeared swiftly by heating up to higher temperatures (i.e., 50 and 75 °C), and the initial orange emission could be resumed within 15 and 5 min, respectively, confirming the capably reversible dual fluorescence switching between blue ($\lambda_{\rm em}$ = 451 nm) and orange ($\lambda_{\rm em}$ = 603 nm) emissions in the prepared PU organogels (see Figure S12c-f, Supporting Information).

It should be noted that the VIE-active fluorophore DPAC has been exploited as fluorescence thermometers, thus optical characteristics of PU-CNC-DDPAC/C organogel were recorded under temperature variations from 0 to 75 °C. As proven in Figure 6a,b, the emission intensity of the orange emission band for PU-CNC-DDPAC/C organogel almost vanished at 0 °C, while the emission intensity of the blue emission band increased concurrently. On the other hand, PU-CNC-DDPAC/C organogel revealed stronger orange fluorescence emissions at high temperatures (i.e., 50 and 75 °C) due to the less constraints of the DPAC unit, providing an efficient strategy to fabricate novel polymeric thermometers possessing ratiometric PL emissions within widespread temperature ranges. Moreover, the PL emission intensity ratios of I_{603}/I_{451} for PU-CNC-DDPAC/C organogel versus various temperatures were plotted in Figure 6c, wherein the relationship between I_{603}/I_{451} and temperatures within the range of 0-75 °C could be depicted by a linear equation with a good correlation coefficient, i.e., y = 0.130x - 0.378, where y: I_{603}/I_{451} ; x:temperature in °C. Besides, PU-CNC-DDPAC/C organogel displayed notably reversible capabilities in PL emission alterations between 0 and 75 °C as shown in Figure 6d, where PL intensity ratios of I₆₀₃/I₄₅₁ exhibited excellent reversibilities up to 10 cycles with negligible decays, recommending prospective exploitations of PU-CNC-DDPAC/C organogel in temperature-sensing applications.

2.5. Rheological Analyses

The mechanical strengths and the stabilities of PU-CNC-RDPAC/1 and PU-CNC-DDPAC/C organogels could be examined by rheological tests. The storage modulus (G') and the

was recorded and shown as Movie S1 in the Supporting Information. However, upon stretching, PU-CNC-DDPAC/E and PU-CNC-RDPAC/2 organogels (containing MIMs after shuttling). i.e., [c2] daisy chain DDPAC/E and [2]rotaxane RDPAC/2, could not demonstrate ratiometric emission color changes as shown in Figure 4c,e and Figure S11a-d (Supporting Information), where the original and major blue emissions at 451 nm remained narrow spans of CIE coordinates in Figure 4c and Figure S11c (Supporting Information), to further ascertain the reduced forcetriggered sliding motions of DPAC stopper moieties to maintain alike constraints of VIE effects. Additionally, the blended PU-CNC(DDPAC/C) organogel (containing freely doped MIMs without shuttling) formed by the physical blending of [c2] daisy chain DDPAC/C (1.5 wt.%) into the standard PU-CNC organogel also could not display dual fluorescence emissions as shown in Figure 4c,f and Figure S11e,f (Supporting Information), where the principal orange emission at 603 nm was still conserved and enclosed in small regions of CIE coordinates (see Figure 4c). Similarly, as observed in Figure 3 and Table 1, not only worse mechanical properties of PU-CNC-DDPAC/E and PU-CNC-RDPAC/2 organogels (containing MIMs after shuttling) along with the blended PU-CNC(DDPAC/C) organogel (containing freely doped MIMs without shuttling) were demonstrated, but also inferior mechano-fluorescent behaviors were verified owing to the lack of sliding motion contributions from these MIM components. The sliding effects of MIM components (acting as artificial muscle moieties) could proficiently dissipate energy to endow PU organogels with greater toughnesses and higher stretchabilities as well as directly alter the distances between slidable macrocycles and DPAC stoppers, thus effectively changing optical performances of DPAC units by reducing their freedom extents upon stretching. As a consequence, the optimum PU-CNC-DDPAC/C organogel containing unconventional [c2] daisy chain rotaxane DDPAC/C acquired the superior mechanical properties than those of containing [2]rotaxane due to more smoothly mutual axles' sliding motions, and yielded the more free suspended states of DPAC stoppers to reveal orange PL emissions in the contracted form (before shuttling) of the unconventional [c2] daisy chain rotaxane owing to its new design of macrocycle-exerted stretching. In particular, diverse local PL spectra taken at different locations in the stretched PU-CNC-DDPAC/C organogel (ca. 3000% strain) were recorded in Figure 5a, wherein various blue to orange emissions ($\lambda_{\rm em}$ = 451 and 603 nm) were evidently observed at certain positions (from A to E) due to possible uneven forces or non-uniform thicknesses. Besides, schematic illustrations of the testing setup for local PL measurements on PU organogels were displayed in Figure 5b,c, where a pinhole of $\emptyset = 0.6$ mm was used to select definite detection areas on the stretched organogel sample to achieve their local PL spectra. Therefore, the effective sliding motions of DPAC stoppers in MIMs as artificial muscle tougheners and in situ molecular shuttling sensors for self-healable mechano-fluorescent PU organogels could be further confirmed by point-by-point detections of the local PL measurements at multiple points, which provided a more comprehensive understanding of these spatial ratiometric emission differences.

Accordingly, to further confirm the ratiometric PL emission switching behaviors, the time-resolved photoluminescence (TRPL) spectra and fluorescence lifetime values of **PU-CNC-**

16163028, 0, Downloaded from https://advanced.onlinelibrary.wiley.com/doi/10.1002/adfm.2025/19737 by Vilnius University, Wiley Online Library on [2210/2025]. See the Terms and Conditions (https://onlinelibrary.wiley.

and-conditions) on Wiley Online Library for rules of use; OA articles are governed by the applicable Creative Commons License

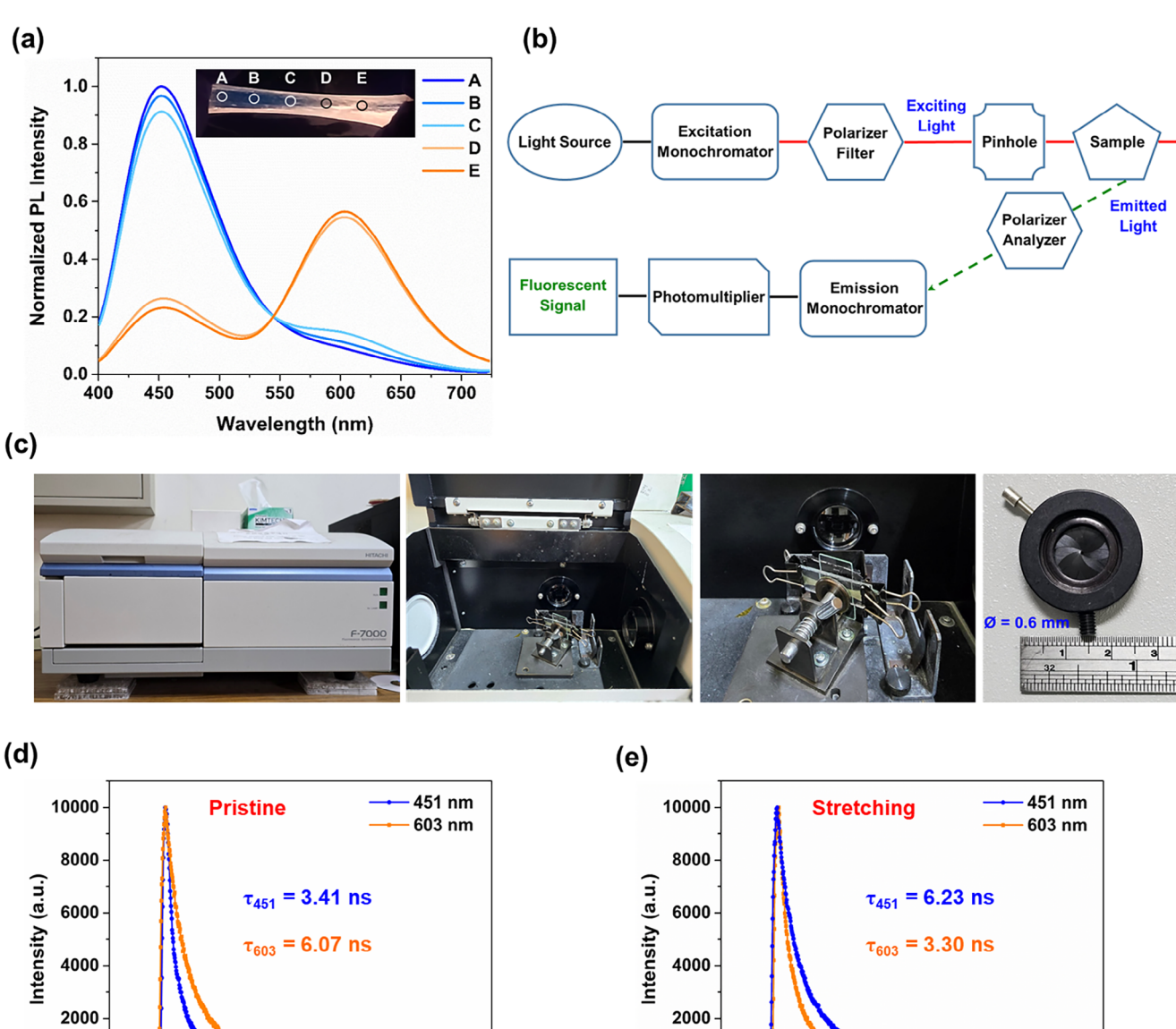


Figure 5. a) Local PL spectra taken at different locations in the stretched PU-CNC-DDPAC/C organogel containing [c2] daisy chain DDPAC/C (contracted form, ca. 3000% strain, $\lambda_{ex} = 365$ nm). b,c) Schematic illustrations and photographs of the testing setup for local PL measurements on PU organogels, wherein a pinhole of $\emptyset = 0.6$ mm was used to select certain detection areas on the sample to achieve point-by-point detections of PL spectra. Inset photo was taken under an UV lamp ($\lambda = 365$ nm). d,e) TRPL profiles of PU-CNC-DDPAC/C organogel before and after stretching ($\lambda_{ex} = 375$ nm, $\lambda_{em} = 451$ and 603 nm).

0

75

80

85

Time (ns)

90

95

loss modulus (*G*") were determined as functions of various parameters, i.e., angular frequency and the strain sweep. In consequence, the angular frequency sweep experiments were proceeded at a constant strain of 1% in the frequency range of 0.1 to 100 rad s⁻¹. As shown in **Figure 7a**,d, the gradual intensifications of *G*' and *G*" values were noticed by increasing frequency from 0.1 to 100 rad s⁻¹ in both **PU-CNC-RDPAC/1** and **PU-CNC-DDPAC/C** organogels. Moreover, *G*' values were found to dominate over *G*" values within the range of 0.1–100 rad s⁻¹

to demonstrate the foundations of stable organogels. Since their storage modulus G' values were over 10³ Pa in frequency sweep experiments, notable mechanical strengths of both organogels could also be confirmed. Furthermore, the strain sweep experiments were conducted with a constant angular frequency of 1 rad s⁻¹ over a wide strain region of 0–1000% strains as performed in Figure 7b,e, wherein storage moduli (G') and loss moduli (G") of PU-CNC-RDPAC/1 and PU-CNC-DDPAC/C organogels were plotted as a function of % strain. It was observed that G'

0

75

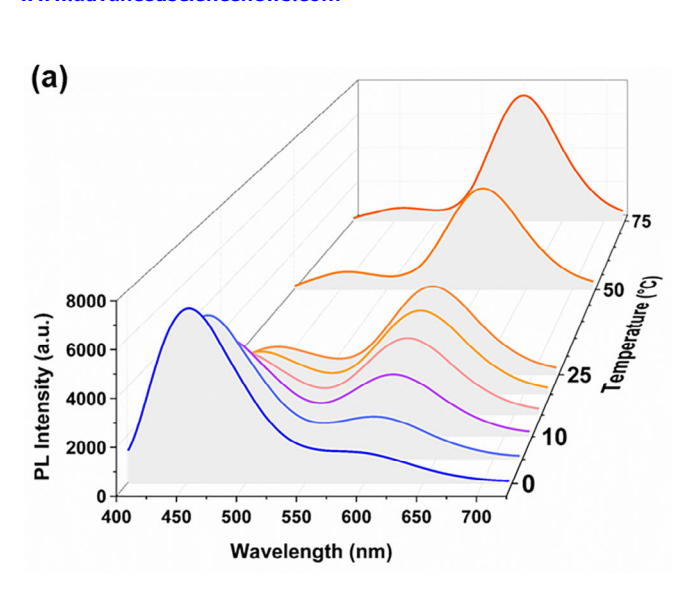
80

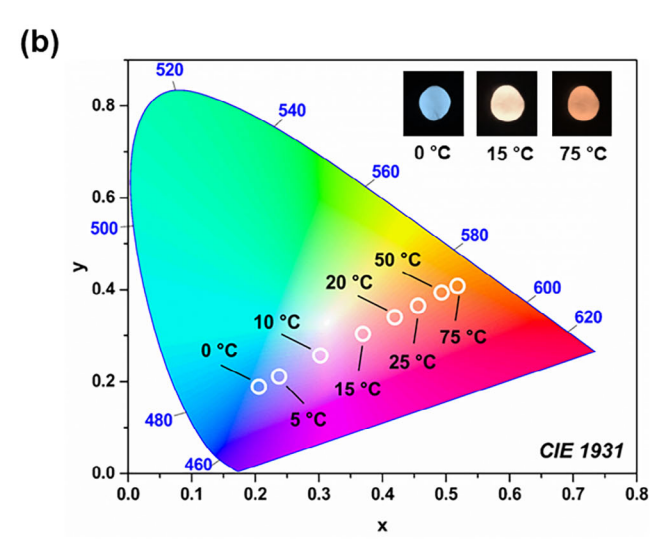
85

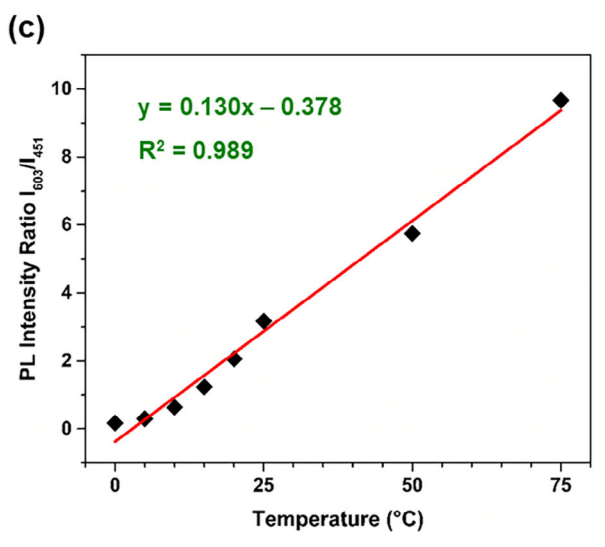
Time (ns)

90

95







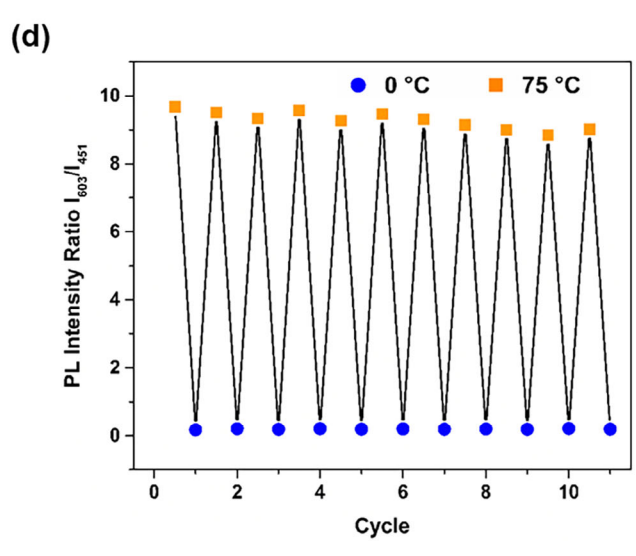


Figure 6. a) PL spectra, b) CIE 1931 coordinates, and c) PL intensity ratios (I_{603}/I_{451}) of orange ($\lambda_{em}=603$ nm) and blue ($\lambda_{em}=451$ nm) emissions for **PU-CNC-DDPAC/C** organogel containing [c2] daisy chain **DDPAC/C** (contracted form) with various temperatures from 0 to 75 °C ($\lambda_{ex}=365$ nm). d) PL intensity ratios (I_{603}/I_{451}) for **PU-CNC-DDPAC/C** organogel upon reversibility tests (ca. 10 cycles) by temperature variations between 0 and 75 °C.

values were higher than G" values, and the fluctuations of G' and G" values were minor within a certain strain range (i.e., linear viscoelastic region) of organogels. However, when the strain reached the values of 200-300%, G' values started to decrease rapidly and dropped below G" values beyond the crossover point ca. 700% strains, indicating the collapses of gel networks under high deformations with the strain values > 700%. Besides, the strain sweep experiments of PU-CNC-RDPAC/1 and PU-CNC-DDPAC/C organogels were complemented with a lower angular frequency of 0.1 rad s⁻¹ over a strain range of 0–1000% strains as shown in Figure S13a,d (Supporting Information), wherein G'/G" crossover points could be obtained ca. 300% strains, confirming that PU organogels tended to behave more like viscous liquids at low frequencies. Additionally, the corresponding low and high strains of 1 and 700% deformations were carried out alternatively at a fixed angular frequency of 10 rad s⁻¹ as presented in Figure 7c,f, in which the restored gel phases of G' > G'' values were acquired at a low strain of 1% after the distortions of gel networks under a larger deformation of 700% strain. Despite being repeated the deformations at the higher strain of 700%, gel networks still could recover to their initial linear viscoelastic regions when the lower strain of 1% was applied, implying that the whole gel networks could be regained completely after a number of damages to ascertain self-healing capabilities of constructed PU-CNC-RDPAC/1 and PU-CNC-DDPAC/C organogels. Also, the relaxation behaviors of PU-CNC-RDPAC/1 and PU-CNC-DDPAC/C organogels were further examined through stress relaxation experiments achieved at room temperature. A shear strain of 1% was applied and the time dependent modulus values G(t) were plotted as a function of time in Figure S13b,e (Supporting Information), in which G(t) values decayed with time, demonstrating the stress relaxations of PU organogels. Afterwards, the temperature dependences of G' and G" moduli for PU-CNC-RDPAC/1 and PU-CNC-DDPAC/C organogels



www.afm-journal.de

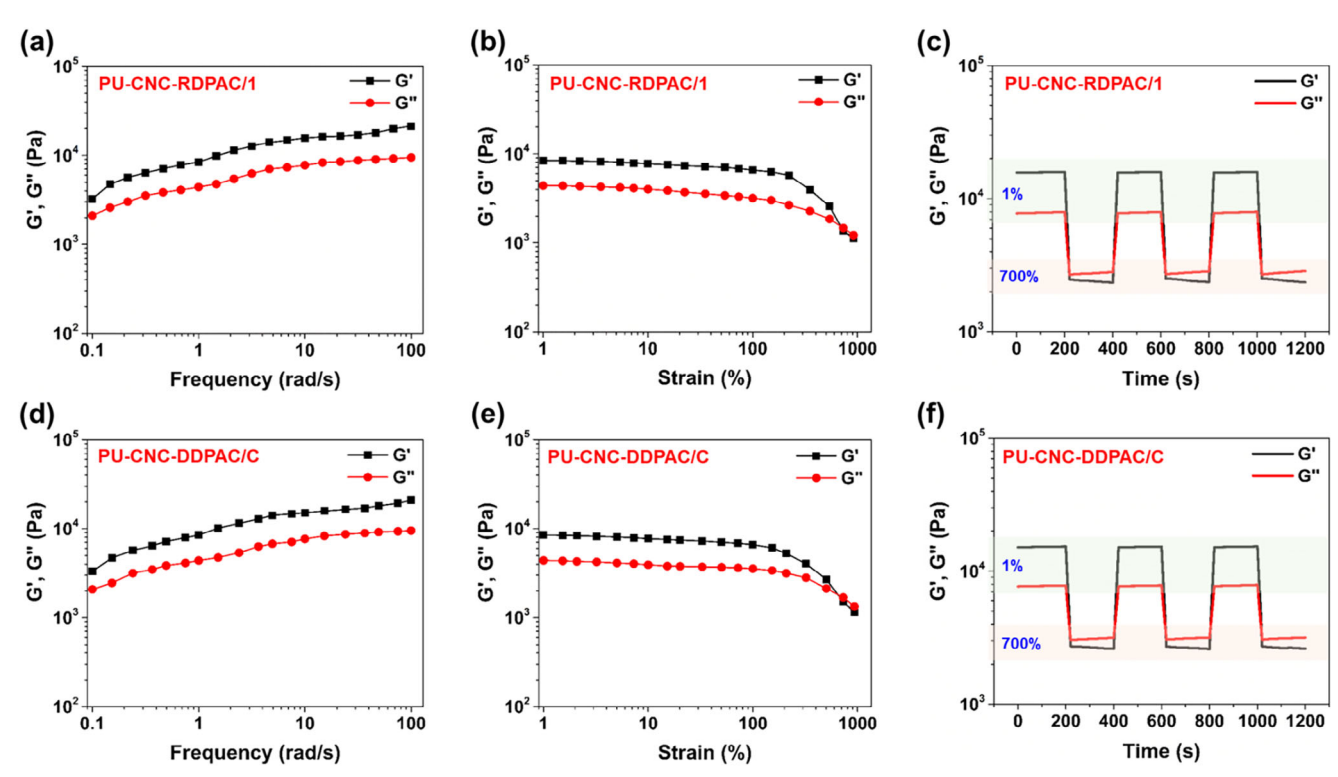


Figure 7. Rheological properties of PU-CNC-RDPAC/1 and PU-CNC-DDPAC/C organogels containing [2] rotaxane RDPAC/1 (before shuttling) and [c2] daisy chain DDPAC/C (contracted form): Dynamic storage (G') and loss (G'') modulus values for a) and d) frequency dependences at 1% strain, b,e) strain dependences with an angular frequency of 1 rad s⁻¹ along with c,f) alternative strain changes at an angular frequency of 10 rad s⁻¹ with oscillation forces of 1 and 700% strains, respectively.

were proven in Figure S13c,f (Supporting Information) during heating processes at a constant heating rate of 5 °C/min. Owing to decreased hydrogen bonds upon heating, both G' and G'' moduli dropped with augmented temperatures from 5 to 80 °C, proposing that heat initiated more efficient destructions of intermolecular interactions in polymer networks, i.e., hydrogen bond breakages.

2.6. X-Ray Diffraction (XRD) Analyses

Other than the macroscopic mechanical tests, small and wide angle X-ray scattering (SAXS and WAXS) measurements were also conducted to survey the microstructures of PU-CNC-DDPAC/C organogel in divergent elongation tests with various stretching ratios (i.e., 2000% and 4000% strains) as shown in Figure S14 (Supporting Information). Without tensile forces, no any obvious peaks could be discerned in the 1D SAXS curve of PU-CNC-DDPAC/C organogel (i.e., 0% strain) as exhibited in Figure S14a (Supporting Information), proposing that PU-CNC-DDPAC/C organogel preserved an amorphous micro-phase separated structure. When the tensile strains were prolonged, hydrogen-bonded segments of hard domains in PU-CNC-DDPAC/C organogel tended to aggregate, resulting in the amplification of 1D SAXS curve with one prominent q value ca. 0.06 Å^{-1} in consequence of the average inter-domain distance of 10.5 nm between oriented microphase-separated domains. Besides, the 2D SAXS patterns of PU-CNC-DDPAC/C organogel in Figure S14c (Supporting Information) revealing a uniform circular shape could be employed to confirm the isotropic structure of PU-CNC-DDPAC/C organogel with random dispersions of hard domains within PU matrices in the un-stretched state (at 0% strain). The scattering circle in Figure S14c (Supporting Information) in the small angle range was gradually deformed to two arcs by increasing tensile strains up to 4000%, signifying that this average inter-domain distance of 10.5 nm in hard segments was continually orientated along the stretching direction, increased orientation degrees of hard domains in the stretching direction could be noticed, and tensile forces could induce aligned microstructures.

Moreover, the 1D WAXS and 2D WAXS profiles of PU-CNC-DDPAC/C organogel under various strains (i.e., 2000% and 4000% strains) shown in Figure S14b,d (Supporting Information) could be used to verify its structural conversions from static to tensile forms. As presented in Figure \$14b (Supporting Information), probably intensified orientations of molecular structures and possible diminutions of thicknesses could occur as the tensile strain up to 4000%. Therefore, the intensity of the scattering peak at $q \approx 15 \text{ nm}^{-1}$ in the wide angle range for PU-CNC-DDPAC/C organogel was decayed, evidencing their π - π stacking and backbone structures with a periodic distance of 4.2 Å. Furthermore, the centralization and transformation into two arcs (with $q \approx 15 \text{ nm}^{-1}$ and a d-spacing value ca. 4.2 Å) in the meridional direction for the initial isotropic scattering halo of 2D WAXS pattern with the enhancing strain could be observed in Figure S14d (Supporting Information), identifying

16163028, Q. Downloaded from https://advanced.online.library.wiley.com/doi/10.1002/adfm.202519737 by Vilnis University, Wiley Online Library on [22102025]. See the Terms and Conditions (https://onlinelibrary.wiley.com/terms-and-conditions) on Wiley Online Library for rules of use; OA articles are governed by the applicable Creative Commons License

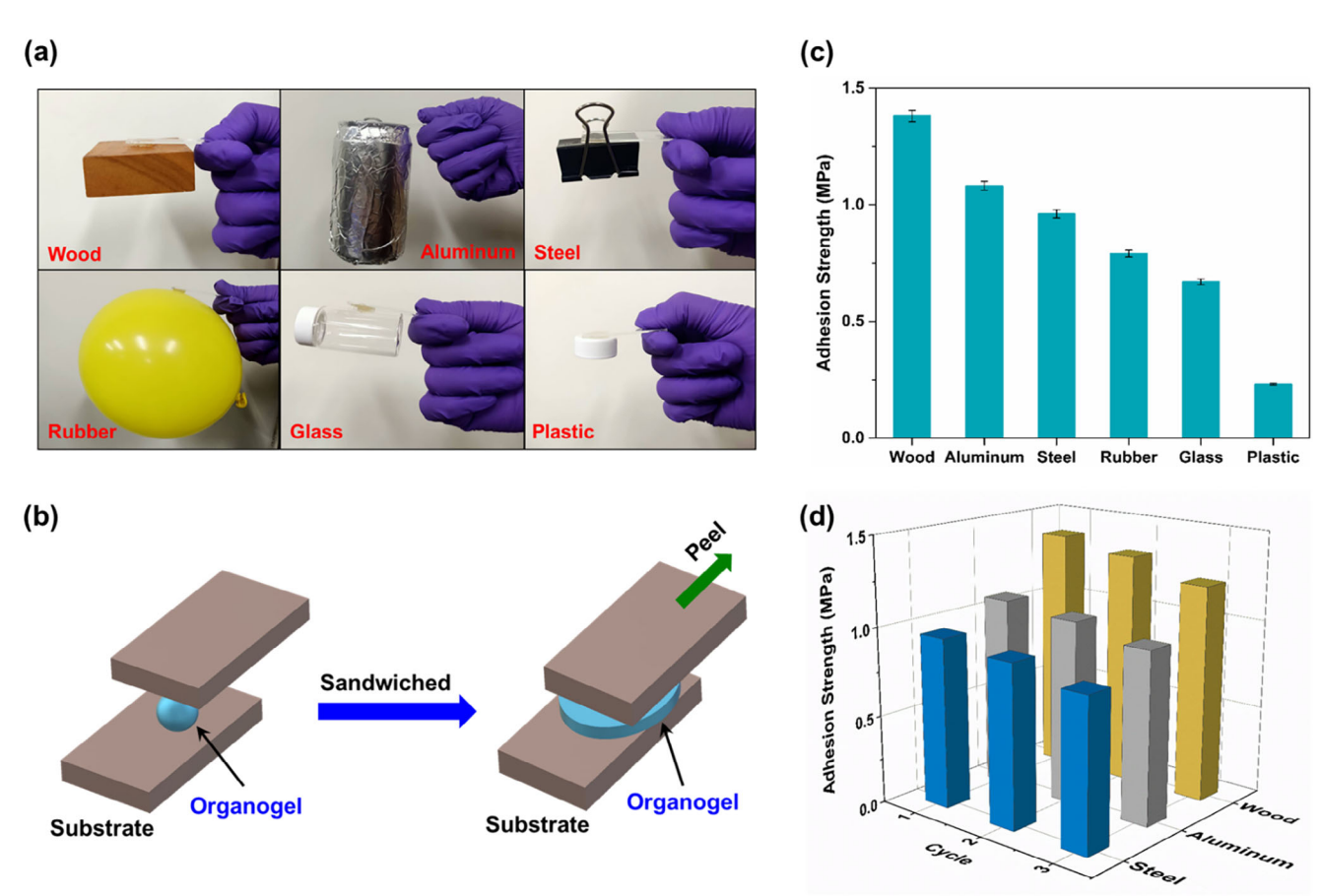


Figure 8. a) Optical images of PU-CNC-DDPAC/C organogel containing [c2] daisy chain DDPAC/C (contracted form) adhered to different substrates. b) Schematic illustrations of shear adhesion tests. c) Maximum shear adhesion strengths of PU-CNC-DDPAC/C organogel adhered to various substrates. d) Repetitive adhesion tests of PU-CNC-DDPAC/C for 3 cycles on 3 diverse substrates (i.e., wood, aluminum, and steel).

that the periodic distance of π - π stacking associated with the favorite arrangements of PU backbones was induced in the perpendicular orientation with respect to the tensile stretching direction. These SAXS and WAXS results affirmed that PU-CNC-DDPAC/C organogel containing the slidable [c2] daisy chain component suggested some specific orientations during stretching, which might be rational reasons for mechanical behaviors of the designed mechano-fluorescent organogels to preserve high toughnesses and large strains. In addition, SAXS and WAXS data of the standard PU-CNC organogels with different amounts of CNCs as cross-linkers, i.e., 0.25, 0.5, 0.75, and 1.0 wt.%, were collected to be shown in Figure S15a,b (Supporting Information), wherein the percolations and alignments of CNCs in PU networks couldn't be distinguished obviously due to very few amounts of CNCs cross-linkers added in PU organogel systems. Likewise, as exhibited in Figure S15c,d (Supporting Information), SAXS and WAXS profiles of PU-CNC (without MIMs) and PU-CNC-DDPAC/C (containing MIMs) organogels before and after stretching of ca. 2500% strains couldn't be employed to clarify evidently the alignments of MIMs in PU matrices during stretching, which might be assigned to the incorporations of minor amounts (1.5 wt.%) of MIMs into PU organogels, leading to the difficult recognition of MIM contributions on the orientations of polymer chains.

2.7. Adhesive, Self-Healing, and Storage Properties

It was found that adhesive properties of polymer gels are evaluated as important issues for the fabrications of stretchable sensors to possess robust interactions with multiple substrates. As verified in Figure 8a, the prepared PU-CNC-DDPAC/C organogel containing cellulose nanocrystals (CNCs) cross-linker to offer multiple hydrogen bonds could facilely adhere to different substrates, i.e., wood, aluminum, steel, rubber, glass, and plastics. Additionally, the quantitative lap shear tests were carried out to estimate adhesion strengths of PU-CNC-DDPAC/C organogel on different substrates, in which PU-CNC-DDPAC/C organogel was sandwiched between two surfaces as shown in Figure 8b. Later on, the surfaces were stretched up to the appearances of separations (adhesive failures) or ruptures (cohesive failures). The quantified values of adhesion strengths on various substrates are depicted in Figure 8c and Figure \$16a (Supporting Information), where PU-CNC-DDPAC/C organogel exhibited quite strong adhesion strengths toward various substrates but preferably stuck to cellulose-type materials (i.e., wood). The adhesive repeatabilities of PU-CNC-DDPAC/C organogel to certain surfaces were also outstanding as there were no remarkable losses of adhesive strengths after 3 times of repeated adhesions in the tensile lap shear tests (see Figure 8d; Figure S16b, Supporting

and-conditions) on Wiley Online Library for rules of use; OA articles are governed by the applicable Creative Commons License

www.afm-journal.de

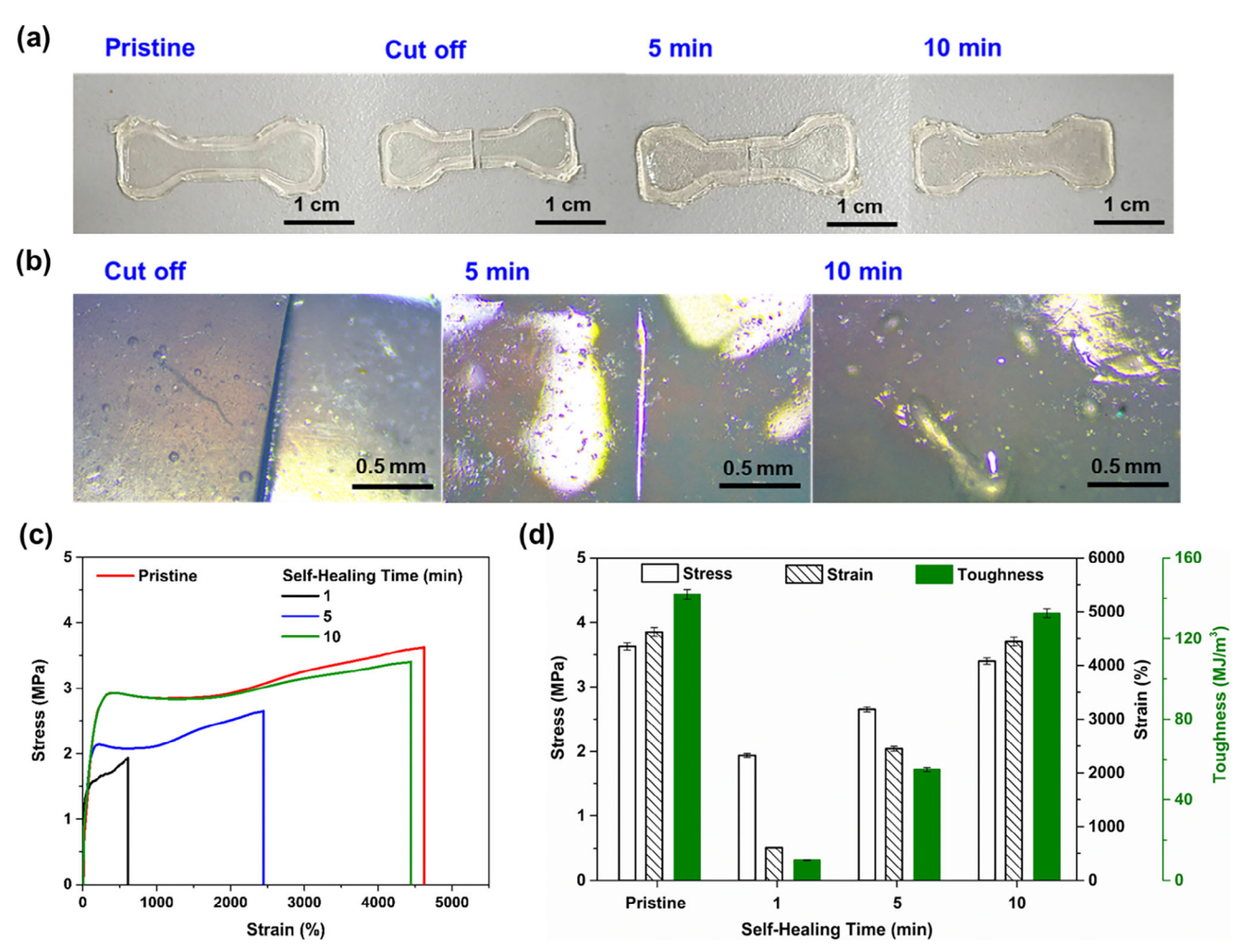


Figure 9. a) Photographs and b) optical microscopic images of the self-healable **PU-CNC-DDPAC/C** organogel containing [c2] daisy chain **DDPAC/C** (contracted form) during the cutting and self-healing processes with different self-healing times (i.e., 5 and 10 min) at room temperature. c) Stress–strain curves and d) stress/strain/toughness histograms of the self-healable **PU-CNC-DDPAC/C** organogel under tensile loading with different self-healing times at room temperature (by using a strain rate of 30 mm s⁻¹).

Information), indicating that the vigorous and repeatable adhesivenesses of PU-CNC-DDPAC/C organogel were primarily due to plentiful reversible hydrogen bonds on organogel-substrates.

Significantly, the adhesive features could support the selfhealing performances of gel materials, thereby self-healing capabilities of PU-CNC-DDPAC/C organogel comprising CNCs cross-linker to generate hydrogen bonding interactions could be directly envisaged in Figure 9. Thoroughly, a dog bone shaped specimen of PU-CNC-DDPAC/C organogel was cut into two pieces, which were mildly pressed together, they could be healed autonomously at room temperature to be stretched again (see Figure 9a). The dynamic self-healing behaviors of PU-CNC-DDPAC/C organogel were further evaluated by using optical microscope images at different stages along with mechanical tests. As shown in Figure 9b, the fracture gap of PU-CNC-DDPAC/C pieces was reduced rapidly, and PU-CNC-DDPAC/C specimen recovered its initial shape within 10 min at room temperature. Also, mechanical properties of PU-CNC-DDPAC/C organogel specimen enhanced with the extended healing time as presented

in Figure 9c,d, wherein the tensile stress of 3.40 MPa and strain of 4445% could be restored (i.e., 93.7% and 96.1% of their original values, respectively) after 10 min of self-healing. The loss of mechanical features after self-healing processes might be due to the incompletely reversible breakages of hydrogen bonds. These results indicated that PU-CNC-DDPAC/C organogel consisting of CNCs cross-linker performed effective self-healing characteristics at room temperature, implying its probable applications in preparing flexible sensors. Furthermore, self-healing behaviors of PU-CNC-DDPAC/C organogel at high temperatures (i.e., 50 and 75 °C) could also be studied as shown in Figure S17 (Supporting Information), wherein more effective and speedy self-healing capabilities of PU-CNC-DDPAC/C organogel could be acquired. As well, mechanical characteristics of the self-healable PU-CNC-DDPAC/C organogel conserved almost identical to those of the pristine PU organogel, even after 10 healing cycles as presented in Figure \$18 (Supporting Information), inferring the excellent re-configurabilites of hydrogen-bonded PU networks in the selfhealing organogels.





www.afm-journal.de

Interestingly, the prepared PU-CNC-DDPAC/C organogel still preserved a large tensile strain of ≈4000%, a high tensile stress of 3.74 MPa, an excellent toughness of ≈ 137 MI m⁻³, and a sturdy adhesive strength of 1.25 MPa toward wood at the ambient storage for 9 days, proposing the great resistance of PU-CNC-DDPAC/C organogel to drying, which could considerably broaden its utilization scenarios (see Figure \$19a,b and Figure \$20a, Supporting Information). Moreover, adhesive features of PU-CNC-DDPAC/C organogel toward wood at distinct temperatures could also be appraised as presented in Figure S20b (Supporting Information), in which adhesive strengths of PU-CNC-DDPAC/C organogel were reduced either at low temperature (i.e., 0 °C) or at high temperatures (i.e., 50 and 75 °C). The possible reasons might be that the adhesive organogel became more brittle at low temperatures, leading to the weak adhesion between the organogel and the substrate, whereas the adhesive organogel became more ductile at high temperatures, making it less robust and more liable to creep. In addition, the dual fluorescence emission behaviors with various storage periods were also investigated as revealed in Figure \$19c,d (Supporting Information), where PU-CNC-DDPAC/C organogel still maintained an orange fluorescence emission at the ambient storage for 9 days. Therefore, the targeted MIM-based PU organogels possessing excellent adhesive, self-healing, and storage properties might be extended for future abundant applications.

3. Conclusion

Distinct force-induced dual PL emission switching of selfhealable PU organogels containing DPAC-based MIMs, i.e., [2]rotaxanes and extended/contracted [c2] daisy chain molecules, with novel shuttling motions as well as multiple hydrogenbonded CNCs cross-linkers were generated by step-growth polymerizations in this study. Interestingly, the incorporation of fairly small amounts (ca. 1.5 wt.%) of MIMs, including [2]rotaxane and daisy chain moieties, in all monomer components could promote mechanical features of obtained PU organogels effectively due to the energy dissipations of MIMs with slidable components as artificial molecular muscles. Therefore, the optimum PU-CNC-DDPAC/C organogel consisting of daisy chain moiety DDPAC/C (contracted form, 1.5 wt.%) in PU scaffolds illustrated the outstanding stretchability to possess the most excellent toughness up to 142 MJ m⁻³ (i.e., \approx 2.6 times tougher than \approx 55 MJ m⁻³ of the standard PU organogel without MIMs), the longest tensile strain over 4600%, and the highest stress of 3.63 MPa (at a high strain rate of 30 mm s⁻¹). More importantly, the attractive ratiometric PL responses of blue ($\lambda_{\rm em}$ = 451 nm) and orange ($\lambda_{\rm em}$ = 603 nm) emissions could be observed in both PU-CNC-RDPAC/1 and PU-CNC-DDPAC/C organogels by integrating DPAC-based [2]rotaxane RDPAC/1 (before shuttling) and daisy chain DDPAC/C (contracted form) moieties into PU frameworks, which enabled innovative dual fluorescence switching behaviors from orange ($\lambda_{\rm em} = 603$ nm) to blue ($\lambda_{\rm em} = 451$ nm) emissions (before and after shuttling) upon tensile force-driven sliding motions of macrocyclic components in MIMs to manipulate VIE effects on ratiometric emissions of freedom-dependent DPAC stoppers. By lacking of sliding motion contributions from MIM components, both of the PU organogels containing MIMs after shuttling (i.e., PU-CNC-DDPAC/E and PU-CNC- RDPAC/2) and the blended organogel containing freely doped MIMs without shuttling, i.e., PU-CNC(DDPAC/C), revealed inferior mechanical properties and worse mechano-fluorescent characteristics in contrast to the optimized analogues of PU-CNC-DDPAC/C organogel (featuring artificial muscle functions with the contracted form before shuttling). Moreover, the optimum PU organogel containing unconventional [c2] daisy chain rotaxane not only yielded the better mechanical properties than those of containing [2]rotaxane due to the more fluently mutual axles' sliding motions, but also gave the more free suspended states of DPAC stoppers to show orange PL emissions in the contracted form (before shuttling) of the unconventional [c2] daisy chain rotaxane owing to its new design of macrocycle-exerted stretching. Notably, the effective sliding motions of DPAC stoppers in MIMs as artificial muscle tougheners and in situ molecular shuttling sensors for self-healable mechano-fluorescent PU organogels could be verified by point-by-point detections of the local PL measurements at multiple points in this study. Furthermore, the rheological tests were also proceeded to explore mechanical strengths and stabilities of PU-CNC-RDPAC/1 and PU-CNC-DDPAC/C organogels (before shuttling). In addition, XRD analyses were utilized to study stretching deformations of PU-CNC-DDPAC/C organogel (contracted form) to verify interrelated morphological properties of stretching states in the oriented MIM-based PU organogels. Accordingly, our designed MIM-based PU organogels (including the optimum PU-CNC-DDPAC/C) revealed prominently adhesive and selfhealing behaviors as well as outstanding storage stabilities to show characteristic force- and temperature-induced fluorescence color responses, assisting potential mechano-fluorescence and temperature sensor applications of multiple functional PU organogels to be employed in various fields of cutting-edge materials.

Supporting Information

Supporting Information is available from the Wiley Online Library or from the author.

Acknowledgements

The authors are grateful for the funding from the National Science and Technology Council of Taiwan (through grant nos. NSTC 113-2221-E-A49-008, NSTC 113-2113-M-A49-014, and NSTC 113-2923-M-A49-006-MY2) and the Research Council of Lithuania (through grant no. P-LT-TW-24-17). Besides, this work is also supported by the Center for Emergent Functional Matter Science of National Yang Ming Chiao Tung University from the Featured Areas Research Center Program within the framework of the Higher Education Sprout Project and the International Integrated Collaboration Project for Interested Czech Universities (ICU) & University Academic Alliance in Taiwan (UAAT) by the Ministry of Education (MOE) in Taiwan. Moreover, the authors would like to thank the Taiwan Light Source (TLS) and Taiwan Photon Source (TPS) beamlines of the National Synchrotron Radiation Research Center (NSRRC) in Hsinchu, Taiwan for providing synchrotron beamtime and technical supports.

Conflict of Interest

The authors declare no conflict of interest.

and Conditions (https://onlinelibrary.wiley

ns) on Wiley Online Library for rules of use; OA articles are governed by the applicable Creative Commons

www.advancedsciencenews.com



www.afm-journal.de

Data Availability Statement

The data that support the findings of this study are available in the supplementary material of this article.

Keywords

mechanically interlocked molecules, N,N'-diphenyl-dihydrodibenzo [a,c]phenazines, polyurethane organogels, ratiometric mechanofluorescence emissions, self-healing behaviors

Received: July 31, 2025 Revised: August 22, 2025 Published online:

- [1] J. F. Stoddart, Angew. Chem., Int. Ed. 2017, 56, 11094.
- [2] D. Sluysmans, Trends Chem. 2019, 1, 185.
- [3] B. T. Shahraki, S. Maghsoudi, Y. Fatahi, N. Rabiee, S. Bahadorikhalili, R. Dinarvand, M. Bagherzadeh, F. Verpoort, *Coord. Chem. Rev.* 2020, 423, 213484.
- [4] A. W. Heard, S. M. Goldup, ACS Cent. Sci. 2020, 6, 117.
- [5] P. Q. Nhien, T. T. K. Cuc, T. M. Khang, C.-H. Wu, B. T. B. Hue, J. I. Wu, B. W. Mansel, H.-L. Chen, H.-C. Lin, ACS Appl. Mater. Interfaces 2020, 12, 47921
- [6] T. T. K. Cuc, P. Q. Nhien, T. M. Khang, C.-C. Weng, C.-H. Wu, B.-t. B. Hue, Y.-K. Li, J. I. Wu, H.-C. Lin, Chem. Mater. 2020, 32, 9371.
- [7] L. Binks, C. Tian, S. D. P. Fielden, I. J. Vitorica-Yrezabal, D. A. Leigh, J. Am. Chem. Soc. 2022, 144, 15838.
- [8] A. S. Baluna, M. Dommaschk, B. Groh, S. Kassem, D. A. Leigh, D. J. Tetlow, D. Thomas, L. V. López, J. Am. Chem. Soc. 2023, 145, 27113.
- [9] M. Gauthier, J. B. M. Whittingham, A. Hasija, D. J. Tetlow, D. A. Leigh, J. Am. Chem. Soc. 2024, 146, 29496.
- [10] E. Moulin, C. C. Carmona-Vargasa, N. Giuseppone, Chem. Soc. Rev. 2023, 52, 7333.
- [11] J.-C. Chang, S.-H. Tseng, C.-C. Lai, Y.-H. Liu, S.-M. Peng, S.-H. Chiu, Nat. Chem. 2017, 9, 128.
- [12] Q. Zhang, S.-J. Rao, T. Xie, X. Li, T.-Y. Xu, D.-W. Li, D.-H. Qu, Y.-T. Long, H. Tian, Chem 2018, 4, 2670.
- [13] C. J. Bruns, J. Li, M. Frasconi, S. T. Schneebeli, J. Iehl, H.-P. J. d. Rouville, S. I. Stupp, G. A. Voth, J. F. Stoddart, *Angew. Chem., Int. Ed.* 2014, 53, 1953.
- [14] C. J. Bruns, M. Frasconi, J. Iehl, K. J. Hartlieb, S. T. Schneebeli, C. Cheng, S. I. Stupp, J. F. Stoddart, J. Am. Chem. Soc. 2014, 136, 4714.
- [15] P. Q. Nhien, J.-H. Tien, T. T. K. Cuc, T. M. Khang, N. T. Trung, C.-H. Wu, B. T. B. Hue, J. I. Wu, H.-C. Lin, J. Mater. Chem. C 2022, 10, 18241.
- [16] N. T. Trung, P. Q. Nhien, T. T. K. Cuc, C.-H. Wu, B. T. B. Hue, J. I. Wu, Y.-K. Li, H.-C. Lin, ACS Appl. Mater. Interfaces 2023, 15, 15353.
- [17] L. Chen, X. Sheng, G. Li, F. Huang, Chem. Soc. Rev. 2022, 51, 7046.
- [18] L. F. Hart, J. E. Hertzog, P. M. Rauscher, B. W. Rawe, *Nat. Rev. Mater.* 2021, 6, 508.
- [19] S. Mena-Hernando, E. M. Pérez, Chem. Soc. Rev. 2019, 48, 5016.
- [20] C. Y. Shi, Q. Zhang, C. Y. Yu, S. J. Rao, S. Yang, H. Tian, D. H. Qu, Adv. Mater. 2020, 32, 2000345.
- [21] X. Zhang, K. Liu, J. Zhao, Z. Zhang, Z. Luo, Y. Guo, H. Zhang, Y. Wang, R. Bai, D. Zhao, X. Yang, Y. Liu, X. Yan, J. Am. Chem. Soc. 2022, 144, 11434.
- [22] J. Zhao, Z. Zhang, L. Cheng, R. Bai, D. Zhao, Y. Wang, W. Yu, X. Yan, J. Am. Chem. Soc. 2022, 144, 872.
- [23] Z. Zhang, J. Zhao, X. Yan, Acc. Chem. Res. 2024, 57, 992.
- [24] Z. Zhang, W. You, P. Li, J. Zhao, Z. Guo, T. Xu, J. Chen, W. Yu, X. Yan, J. Am. Chem. Soc. 2023, 145, 567.

- [25] S.-W. Zhou, D. Zhou, R. Gu, C.-S. Ma, C. Yu, D.-H. Qu, *Nat. Commun.* 2024, 15, 1690.
- [26] Y. Wang, G. Liu, J. Zhao, Z. Zhang, H. Zhang, Y. Ding, X. Zhang, Z. Liu, W. Yu, X. Yan, Angew. Chem., Int. Ed. 2024, 63, 202409705.
- [27] Z. Luo, X. Zhang, J. Zhao, R. Bai, C. Wang, Y. Wang, D. Zhao, X. Yan, Angew. Chem., Int. Ed. 2023, 62, 202306489.
- [28] J. Zhao, M. Hong, Z. Ju, X. Yan, Y. Gai, Z. Liang, Angew. Chem., Int. Ed. 2022, 61, 202214386.
- [29] D. Zhao, Z. Zhang, J. Zhao, K. Liu, Y. Liu, Gu. Li, X. Zhang, R. Bai, X. Yang, X. Yan, Angew. Chem., Int. Ed. 2021, 60, 16224.
- [30] B. A. Versaw, T. Zeng, X. Hu, M. J. Robb, J. Am. Chem. Soc. 2021, 143, 21461.
- [31] Y. Chen, G. Mellot, D. v. Luijk, C. Creton, R. P. Sijbesma, Chem. Soc. Rev. 2021, 50, 4100.
- [32] W. Qiu, J. M. P. Scofield, P. A. Gurr, G. G. Qiao, Macromol. Rapid Commun. 2022, 43, 2100866.
- [33] T. Watabe, H. Otsuka, Angew. Chem., Int. Ed. 2023, 62, 202216469.
- [34] M. E. McFadden, M. J. Robb, J. Am. Chem. Soc. 2019, 141, 11388.
- [35] J. M. Clough, J. v. d. Gucht, T. E. Kodger, J. Sprakel, Adv. Funct. Mater. 2020, 30, 2002716.
- [36] S. Zhang, C. Sun, J. Zhang, S. Qin, J. Liu, Y. Ren, L. Zhang, W. Hu, H. Yang, D. Yang, Adv. Funct. Mater. 2023, 33, 2305364.
- [37] W. Wang, R. Li, S. Xiao, Q. Xing, X. Yan, J. Zhang, X. Zhang, H. Lan, T. Yi, CCS Chem 2022, 4, 899.
- [38] J. Yang, J. Qin, P. Geng, J. Wang, M. Fang, Z. Li, Angew. Chem., Int. Ed. 2018, 57, 14174.
- [39] Y. Sagara, K. Kubo, T. Nakamura, N. Tamaoki, C. Weder, Chem. Mater. 2017, 29, 1273.
- [40] F. Xie, T. Zhang, P. Bryant, V. Kurusingal, J. M. Colwell, B. Laycock, Prog. Polym. Sci. 2019, 90, 211.
- [41] R. Guo, Q. Zhang, Y. Wu, H. Chen, Y. Liu, J. Wang, X. Duan, Q. Chen, Z. Ge, Y. Zhang, Adv. Mater. 2023, 35, 2212130.
- [42] Y. Zhu, Y. He, W. Lu, H. Tian, F. Fei, P. Zhou, J. Wang, J. Mater. Chem. A 2024, 12, 28716.
- [43] A. Khan, C.-F. Wang, R. R. Kisannagar, W.-T. Chuang, P. Q. Nhien, S. Mahmood, M. Katiyar, D. Gupta, K.-H. Wei, H.-C. Lin, J. Mater. Chem. A 2023, 11, 305
- [44] T. Yamakado, S. Saito, J. Am. Chem. Soc. 2022, 144, 2804.
- [45] K. Suga, T. Yamakado, S. Saito, J. Am. Chem. Soc. 2023, 145, 26799
- [46] H. Hu, X. Cheng, Z. Ma, R. P. Sijbesma, Z. Ma, J. Am. Chem. Soc. 2022, 144, 9971.
- [47] S. Thazhathethil, T. Muramatsu, N. Tamaoki, C. Weder, Y. Sagara, Angew. Chem., Int. Ed. 2022, 61, 202209225.
- [48] Y. Sagara, M. Karman, E. Verde-Sesto, K. Matsuo, Y. Kim, N. Tamaoki, C. Weder, J. Am. Chem. Soc. 2018, 140, 1584.
- [49] T. Muramatsu, Y. Sagara, H. Traeger, N. Tamaoki, C. Weder, ACS Appl. Mater. Interfaces 2019, 11, 24571.
- [50] Y. Sagara, M. Karman, A. Seki, M. Pannipara, N. Tamaoki, C. Weder, ACS Cent. Sci. 2019, 5, 874.
- [51] T. Muramatsu, Y. Okado, H. Traeger, S. Schrettl, N. Tamaoki, C. Weder, Y. Sagara, J. Am. Chem. Soc. 2021, 143, 9884.
- [52] T. M. Khang, R. Huang, A. Khan, W.-T. Chuang, P. Q. Nhien, T. T. K. Cuc, B. T. B. Hue, K.-H. Wei, Y.-K. Li, H.-C. Lin, ACS Materials Lett 2022, 4, 2537.
- [53] T. T. K. Cuc, C.-H. Hung, T.-C. Wu, P. Q. Nhien, T. M. Khang, B. T. B. Hue, W.-T. Chuang, H.-C. Lin, Chem. Eng. J. 2024, 485, 149694.
- [54] T. T. K. Cuc, Y.-C. Tso, T.-C. Wu, P. Q. Nhien, T. M. Khang, B. T. B. Hue, W.-T. Chuang, H.-C. Lin, J. Mater. Chem. C 2024, 12, 14469.
- [55] a) Y. Zhou, L. Li, Z. Han, Q. Li, J. He, Q. Wang, Chem. Rev. 2023, 123, 558; b) Y. Peng, S. Gu, Q. Wu, Z. Xie, J. Wu, Acc. Mater. Res. 2023, 4, 323; c) B. Li, P.-F. Cao, T. Saito, A. P. Sokolov, Chem. Rev. 2023, 123, 701
- [56] F. Han, S. Chen, F. Wang, M. Liu, J. Li, H. Liu, Y. Yang, H. Zhang, D. Liu, R. He, W. Cao, X. Qin, F. Xu, Adv. Sci. 2025, 12, 2412726.





www.afm-journal.de

- [57] Z. Zhang, A. Yao, P. Raffa, Adv. Funct. Mater. 2024, 34, 2407529.
- [58] L. Tian, T. Liu, Y. Jiang, B. He, H. Hao, Chem. Eng. J. 2024, 497, 154890.
- [59] X. Fan, L. Zhang, F. Dong, H. Liu, X. Xu, Carbohydr. Polym. 2023, 308, 120654.
- [60] Y. Guo, X. An, X. Qian, ACS Appl. Mater. Interfaces 2023, 15, 19362.
- [61] S. Yoon, J. H. Choi, B. J. Sung, J. Bang, T. A. Kim, NPG Asia Mater 2022, 14, 61.
- [62] Y. Deng, Y. Yuan, Y. Chen, CCS Chem 2020, 2, 1316.
- [63] Z. Liu, H. K. Bisoyi, Y. Huang, M. Wang, H. Yang, Q. Li, Angew. Chem., Int. Ed. 2022, 61, 202115755.
- [64] C. Xu, Y. Chen, S. Zhao, D. Li, X. Tang, H. Zhang, J. Huang, Z. Guo, W. Liu, Chem. Rev. 2024, 124, 10435.
- [65] M. A. Kuzina, D. D. Kartsev, A. V. Stratonovich, P. A. Levkin, Adv. Funct. Mater. 2023, 33, 2301421.
- [66] H. Chen, F. Yang, Q. Chen, J. Zheng, Adv. Mater. 2017, 29, 1606900.
- [67] F. Yang, X. Li, Y. Chen, Adv. Optical Mater. 2022, 10, 2102552.
- [68] Z. Wei, J. H. Yang, J. Zhou, F. Xu, M. Zrínyi, P. H. Dussault, Y. Osada, Y. M. Chen, Chem. Soc. Rev. 2014, 43, 8114.
- [69] H. Yin, F. Liu, T. Abdiryim, X. Liu, ACS Materials Lett 2023, 5, 1787.
- [70] D. Yan, Z. Wang, Z. Zhang, Acc. Chem. Res. 2022, 55, 1047.
- [71] S. Yang, Y. Yang, X. Xia, B. Zou, B. Wang, Y. Zhang, Adv. Funct. Mater. 2024, 34, 2400500.
- [72] a) F. Zhao, M. Liu, H. Guo, Y. Wang, Y. Zhang, M. He, Z. Cai, Prog. Mater. Sci. 2025, 148, 101355; b) F. Han, X. Xie, T. Wang, C. Cao, J. Li, T. Sun, H. Liu, S. Geng, Z. Wei, J. Li, F. Xu, Adv. Healthcare Mater. 2023, 12, 2201730.
- [73] a) H. Kim, G. Zan, Y. Seo, S. Lee, C. Park, Adv. Funct. Mater. 2024, 34, 2308703; b) Y. Peng, J. Ma, Y. Zhao, D. You, Y. Yao, Z. Deng, J. Liao, Y. Chang, W. Shen, M. Li, R. He, L. Zhou, Adv. Funct. Mater. 2025, 35, 2420311.
- [74] J. Zhang, B. He, Y. Hu, P. Alam, H. Zhang, J. W. Y. Lam, B. Z. Tang, Adv. Mater. 2021, 33, 2008071.
- [75] Y. Huang, L. Ning, X. Zhang, Q. Zhou, Q. Gong, Q. Zhang, Chem. Soc. Rev. 2024, 53, 1090.
- [76] X. Hu, B. Fang, P. Li, J. Wang, J. Li, Y. Dai, M. Yin, Adv. Funct. Mater. 2025, 35, 2423793.
- [77] D. Hu, W. Xu, G. Wang, K. Liu, Z. Wang, Q. Shi, S. Lin, Z. Liu, Y. Fang, Adv. Funct. Mater. 2022, 32, 2207895.

- [78] H. Wu, W. Wu, L. Hu, J. Zhu, Q. Li, Y. Gao, Y. Wei, G. Jiang, Y. Yang, Chem. Eng. J. 2023, 469, 143781.
- [79] K. Liu, K. Liu, S. Hao, A. Hou, J. Cao, M. Quan, Y. Wang, C. Wolverton, J. Zhao, Q. Liu, Adv. Funct. Mater. 2024, 34, 2309296.
- [80] F. Han, T. Wang, G. Liu, H. Liu, X. Xie, Z. Wei, J. Li, C. Jiang, Y. He, F. Xu, Adv. Mater. 2022, 34, 2109055.
- [81] X. Qiu, Q. Cui, Q. Guo, T. Zhou, X. Zhang, M. Tian, Small 2022, 18, 2107164.
- [82] T. M. Khang, P. Q. Nhien, T. T. K. Cuc, C.-C Weng, C.-H. Wu, J. I. Wu, B. T. B. Hue, Y.-K. Li, H.-C. Lin, Small 2022, 19, 2205597.
- [83] K. Fujita, Y. Urano, Chem. Rev. 2024, 124, 4021.
- [84] W. Chen, C.-L. Chen, Z. Zhang, Y.-A. Chen, W.-C. Chao, J. Su, H. Tian, P.-T. Chou, J. Am. Chem. Soc. 2017, 139, 1636.
- [85] Z. Zhang, G. Sun, W. Chen, J. Su, H. Tian, Chem. Sci. 2020, 11, 7525.
- [86] Z. Zhang, X. Jin, X. Sun, J. Su, D.-H. Qu, Coord. Chem. Rev. 2022, 472, 214768.
- [87] Z. Zhang, W. Song, J. Su, H. Tian, Adv. Funct. Mater. 2020, 30, 1902803.
- [88] X. Jin, S. Guo, X. Wang, M. Cong, J. Chen, Z. Zhang, J. Su, D.-H. Qu, H. Tian, Angew. Chem., Int. Ed. 2023, 62, 202305572.
- [89] Z. Zhou, D.-G. Chen, M. L. Saha, H. Wang, X. Li, P.-T. Chou, P. J. Stang, J. Am. Chem. Soc. 2019, 141, 5535.
- [90] W. Chen, C. Guo, Q. He, X. Chi, V. M. Lynch, Z. Zhang, J. Su, H. Tian, J. L. Sessler, J. Am. Chem. Soc. 2019, 141, 14798.
- [91] Z. Zong, Q. Zhang, S.-H. Qiu, Q. Wang, C. Zhao, C.-X. Zhao, H. Tian, D.-H. Qu, Angew. Chem., Int. Ed. 2022, 61, 202116414.
- [92] Z. Huang, T. Jiang, J. Wang, X. Ma, H. Tian, Angew. Chem., Int. Ed. 2021, 60, 2855.
- [93] J. Zhu, L. Liu, X. Chen, X. Jin, Z. Qiu, Q. Wang, J. Su, L. Guo, Z. Zhang, ACS Mater. Lett. 2022, 4, 1462.
- [94] N. T. Trung, C.-H. Chiu, T. T. K. Cuc, T. M. Khang, S. Jalife, P. Q. Nhien, B. T. B. Hue, J. I. Wu, Y.-K. Li, H.-C. Lin, Adv. Mater. 2024, 36, 2311789
- [95] W.-T. Xu, X. Li, P. Wu, W.-J. Li, Y. Wang, X.-Q. Xu, X.-Q. Wang, J. Chen, H.-B. Yang, W. Wang, Angew. Chem., Int. Ed. 2024, 63, 202319502.
- [96] Y. Zhang, Y. Li, H. Wang, Z. Zhang, Y. Feng, Q. Tian, N. Li, J. Mei, J. Su, H. Tian, ACS Appl. Mater. Interfaces 2019, 11, 39351.
- [97] F. Gu, Y. Li, T. Jiang, J. Su, X. Ma, CCS Chem 2022, 4, 3014.